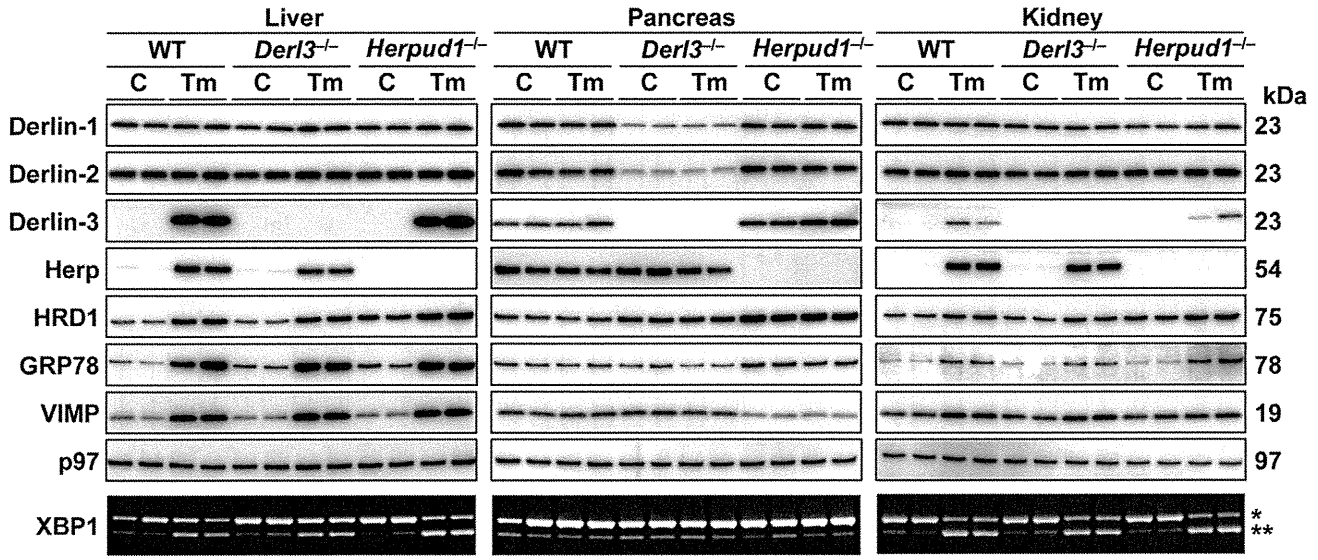

Figure 3. Effects of Derlin-3 and Herp deficiency on the levels of ERAD-related proteins. WT, *Derl3*$^{-/-}$, and *Herpud1*$^{-/-}$ mice were intraperitoneally injected with PBS as control (C) or Tm (2 μg/g body weight) 12 h before sacrifice. Liver, pancreas, and kidney homogenates were subjected to Western blotting using the indicated antibodies. Quantitative data are shown in Figure S2. Total RNAs prepared from the organs were subjected to RT-PCR in order to analyze the splicing of XBP1 (lowest panels). Quantitative data on the ratios (spliced/unspliced+spliced) are shown in Figure 4. *unspliced and **spliced forms of XBP1 mRNA.
doi:10.1371/journal.pone.0034298.g003

post-translational because their mRNA levels were not decreased by Derlin-3 deficiency (compare Figures S2 and 4). The increased protein levels of HRD1 in the *Herpud1*$^{-/-}$ pancreas and kidney may indicate its resistance to Herp-dependent degradation as is the case in the liver. The inconsistency in the protein and mRNA levels of ERAD-related factors may be reflective of the complex, systemic, and organ-specific regulation of each protein at the level of transcription, translation, co-/post-translational modification, and degradation.

Effect of Herp Deficiency on ERAD Substrate Degradation

Partial loss and quantitative imbalance in ERAD-related factors were expected to affect the function of ERAD. Then, we utilized a hydrodynamics-based *in vivo* gene transfection technique, to observe the degradation of ERAD substrates in mice. This technique provides introduction and expression of exogenous genes in whole animals, especially in the liver [31]. We injected a plasmid DNA encoding NHK with a C-terminal green fluorescent protein (GFP) tag to *Herpud1*$^{+/+}$ and *Herpud1*$^{-/-}$ mice. NHK, a truncated mutant of human α1-antitrypsin mainly produced by liver cells, and NHK-GFP are well-characterized as model substrates for ERAD [32,33,34,35,36]. Herp participates in the degradation of NHK in HeLa cells [10]. Western blotting of the *Herpud1*$^{+/+}$ liver expressing NHK-GFP detected the expected band of NHK-GFP, and its levels were elevated by proteasome inhibition (Figure 5A). The exogenous expression of NHK-GFP in the *Herpud1*$^{+/+}$ liver produced not only the intact band but also its fragment bands (Figure 5B), suggesting that NHK-GFP is degraded by ERAD in the mouse liver. In contrast, in the *Herpud1*$^{-/-}$ liver, the levels of the fragment bands were decreased with the accumulation of the intact band. These results indicated that Herp deficiency led to a partial defect in ERAD at least in the liver. Similarly, the other organs of *Herpud1*$^{-/-}$ mice and of *Derl3*$^{-/-}$ mice may also have some defect in ERAD. In that case, *Herpud1*$^{-/-}$ and *Derl3*$^{-/-}$ mice were expected to exhibit abnormality in challenge tests.

Glucose Tolerance and Insulin Response

The changes in ERAD-related proteins and defect in ERAD may induce some systemic phenotypes in Derlin-3– and Herp-deficient mice, especially under stressful conditions. Then, we compared tolerance to conditions associated with ER stress between *Derl3*$^{+/+}$ and *Derl3*$^{-/-}$ and between *Herpud1*$^{+/+}$ and *Herpud1*$^{-/-}$ mice. We performed a glucose tolerance test, because blood glucose levels are a good index of vulnerability to ER stress [37,38]. After glucose was intraperitoneally injected in fasted mice, blood glucose levels in the tails were measured over time (Figure 6). At all time points examined, blood glucose levels in *Derl3*$^{-/-}$ mice were quite similar to those of *Derl3*$^{+/+}$ mice (Figure 6A). In contrast, although blood glucose levels in *Herpud1*$^{-/-}$ mice were normal before glucose administration, *Herpud1*$^{-/-}$ mice showed significantly higher levels of blood glucose than *Herpud1*$^{+/+}$ mice after glucose administration (Figure 6B). Because blood glucose levels were normal in *Herpud1*$^{-/-}$ mice after insulin injections (Figure 6C), Herp deficiency does not appear to cause aberrant responses to insulin. These results indicated that glucose tolerance was impaired not in *Derl3*$^{-/-}$ mice but in *Herpud1*$^{-/-}$ mice. Hyperglycemia has been reported in PERK- [39] and IRE1α-deficient mice [40], both of which are UPR trigger proteins that sense ER stress. Our finding in *Herpud1*$^{-/-}$ mice is the first case of abnormal glucose homeostasis caused by genetic disruption of one UPR target protein contained in ERAD complexes.

Cerebral Infarction Model

ER stress is induced in ischemic areas of the cerebrum, in which an infarction area forms as a result of lethal stress to neuronal cells [41,42]. Herp contributes to protecting neural cells against ER stress-induced apoptosis *in vitro* [21,22]. In this study, to examine the effects of Herp deficiency on resistance to cerebral ischemia *in vivo*, we measured the size of infarct lesions after three-vessel occlusion to cause temporary focal ischemia limited in the neocortex (Figure 7). Twenty-four hours after a 30-min ischemic period, infarction volumes were significantly larger in the

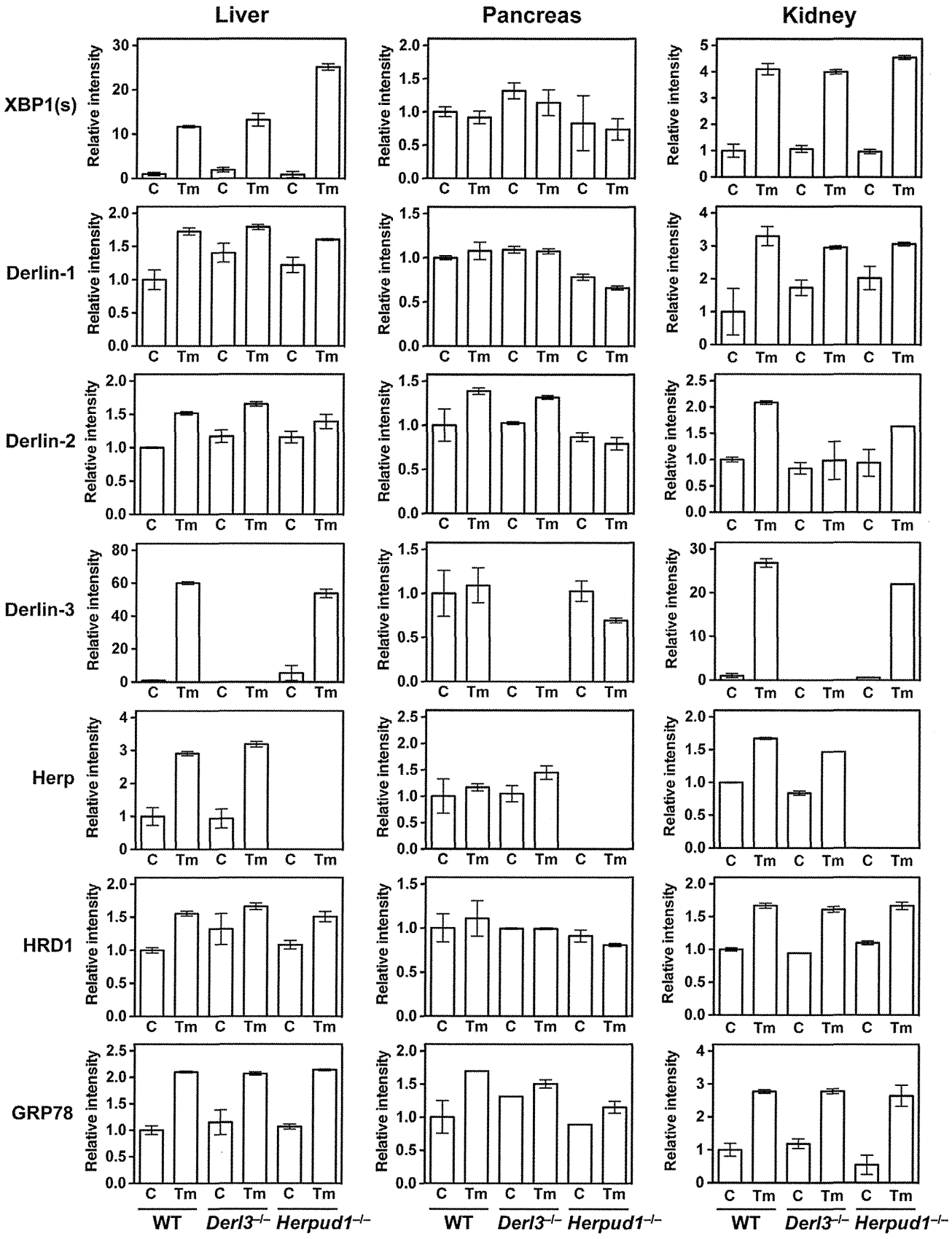

Figure 4. RT-PCR analysis of liver, pancreas, and kidneys from wild-type (WT), *Derl3*$^{-/-}$, and *Herpud1*$^{-/-}$ mice. Mice were intraperitoneally injected with PBS as control (C) or Tm (2 μg/g body weight) 12 h before sacrifice. Total RNAs were prepared from the liver, pancreas, and kidneys and subjected to RT-PCR. The products were analyzed by gel electrophoresis, followed by staining with SYBR Green I. Each band intensity was normalized to the mean intensity for PBS-injected WT mice. Data are expressed as means with range ($n = 2$). XBP1 (s); spliced form of XBP1 mRNA.
doi:10.1371/journal.pone.0034298.g004

neocortices of *Herpud1*$^{-/-}$ mice compared with *Herpud1*$^{+/+}$ mice, indicating that Herp mediates resistance to the cerebral ischemia and reperfusion, probably via increasing resistance of the ER to ischemia-derived ER stress.

In summary, our study demonstrated that Derlin-1–deficient mice were embryonically lethal at much earlier stages (E7–E8), in contrast to HRD1- and Derlin-2–deficient mice, which die at E13.5 [28] and perinatally [29], respectively. At present, it is not clear whether the embryonic death of *Derl1*$^{-/-}$ mice is caused by a defect in ERAD function or by a loss of some as-yet uncharacterized function of the gene. We also showed that Derlin-3– and Herp-deficient mice were born and grew normally, but exhibited some changes in ERAD-related protein components in the liver, pancreas, and kidneys. In addition, the *in vivo* challenge tests indicated that Herp plays a protective role under certain stressful conditions to the ER. These mice may be useful for investigations of the physiological contribution of ERAD under stressful or pathological conditions such as diabetes and ischemia.

Materials and Methods

Ethics Statement

All live mouse experiments were approved by the Animal Care and Use Committee of the National Cerebral and Cardiovascular Center (approval number: 11019), and were performed in accordance with institutional and national guidelines and regulations.

Generation of Knockout Mice

F1 heterozygous mice, *Derl1*$^{+/-}$ and *Derl3*$^{+/-}$, were generated from C57BL/6J-derived Bruce-4 embryonic stem cells (Millipore), and crossed to wild-type C57BL/6JJcl mice (CLEA Japan) for breeding. *Herpud1*$^{+/-}$ mice were generated from 129/SvJ-derived Go Germline embryonic stem cells (Incyte Genomics), and backcrossed to wild-type C57BL/6CrSlc mice (Japan SLC) for 10 generations. Targeting strategies for each gene are shown in Figure 1. The genotypes of offspring were examined by PCR analysis of DNA isolated from ear biopsy. The primer sequences and product sizes are listed in Table S1.

Analysis of Embryos

In crosses of *Derl1*$^{+/-}$ mice, embryos were microscopically isolated from uteri 7, 8, or 10 days after successful copulation, and

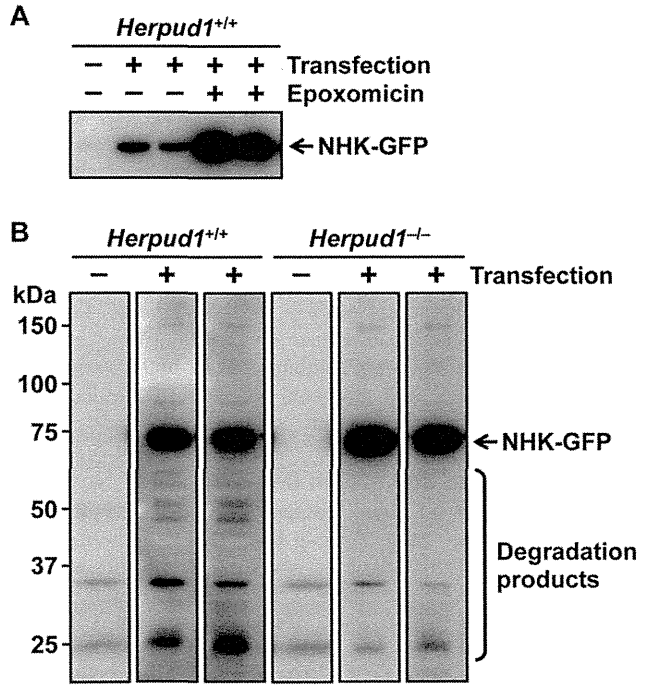

Figure 5. Effect of Herp deficiency on NHK-GFP degradation. (**A**) NHK-GFP was expressed in the livers of *Herpud1*$^{+/+}$ mice in the absence or presence of epoxomicin ($n=2$), and detected by Western blotting using anti-GFP antibodies. (**B**) NHK-GFP was expressed in the livers of *Herpud1*$^{+/+}$ and *Herpud1*$^{-/-}$ mice ($n=2$), and detected by Western blotting using anti-GFP antibodies.
doi:10.1371/journal.pone.0034298.g005

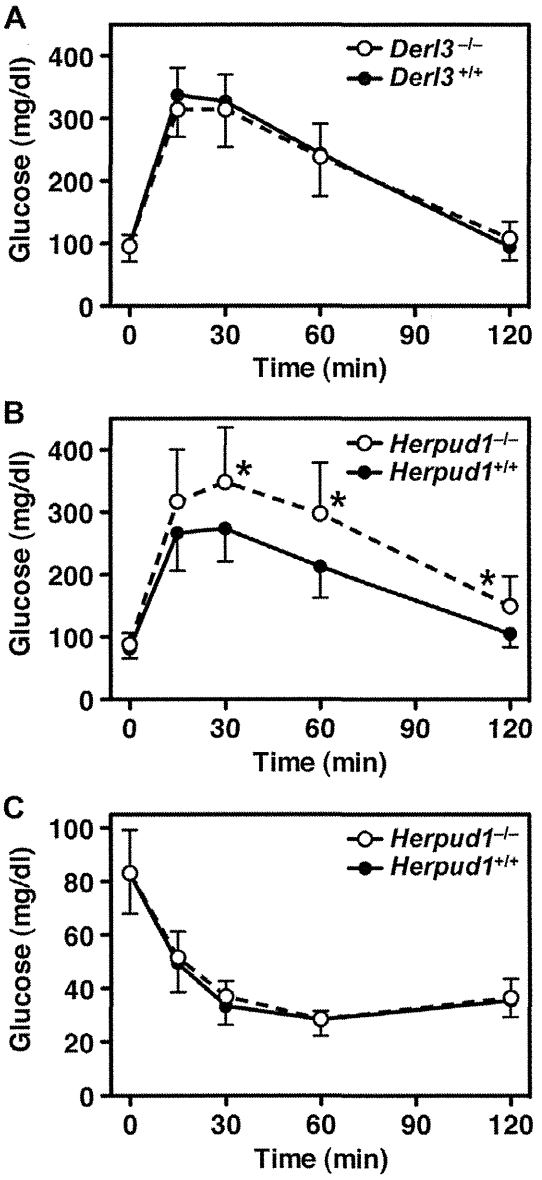

Figure 6. Glucose tolerance and insulin response tests. Blood glucose levels were examined at the indicated time points after intraperitoneal injection of glucose (**A** and **B**) or insulin (**C**) into *Derl3*$^{-/-}$ (**A**, open symbols), *Derl3*$^{+/+}$ (**A**, filled symbols), *Herpud1*$^{-/-}$ (**B** and **C**, open symbols), and *Herpud1*$^{+/+}$ mice (**B** and **C**, filled symbols). Data are expressed as the means with error bars of standard deviation (**A**, $n=12$; **B**, $n=18$; **C**, $n=16$). Asterisks indicate $p<0.01$ (t-test) for *Herpud1*$^{-/-}$ vs. *Herpud1*$^{+/+}$ mice.
doi:10.1371/journal.pone.0034298.g006

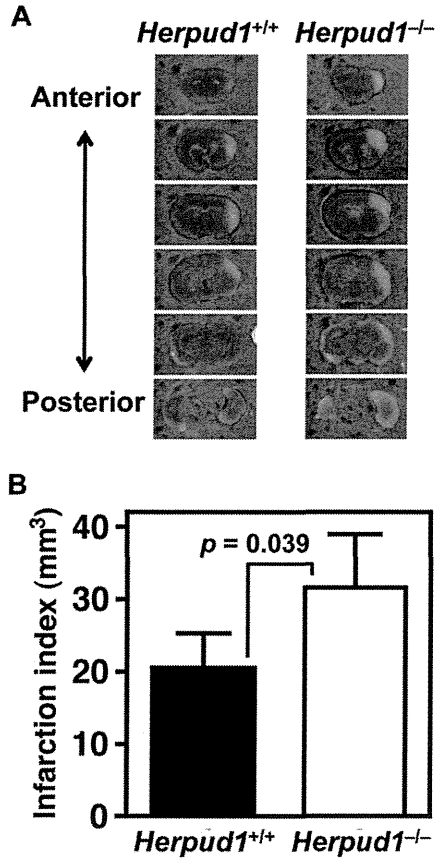

Figure 7. Cerebral infarction models. Neocortical infarction was induced using the temporary three-vessel occlusion method. Representative images of cerebral infarctions from *Herpud1*$^{+/+}$ and *Herpud1*$^{-/-}$ mice stained with 2,3,5-triphenyl-tetrazolium chloride 24 h after ischemia are shown (**A**). White areas indicate infarct regions. Infarction volumes ($n = 6$) are expressed as the means with error bars of standard deviation (**B**).
doi:10.1371/journal.pone.0034298.g007

the developmental stages were confirmed by appearance. The genotypes of embryos were determined by PCR as described above. To increase gestation efficiency, *Derl1*$^{+/-}$ mice with mixed genetic backgrounds, C57BL/6JJcl and Jcl:ICR (CLEA Japan), were used for the embryonic studies.

Tissue Preparation

To examine the effects of pharmacologically induced ER stress *in vivo*, 18-h fasted male mice were intraperitoneally injected with PBS or tunicamycin (WAKO, 200 μg/ml dissolved in PBS) at a dose of 2 μg/g body weight. After 12 h, the anesthetized mice were perfused with PBS, and their liver, pancreas, and kidneys were excised. The organ tissues were homogenized by Polytron PT1200 (Kinematica) in SDS-PAGE sample buffer. Tissue homogenates were subjected to Western blotting. Equal loading of the samples was confirmed by quantitating protein levels in gels stained with GelCode Blue Stain Reagent (Thermo Scientific). Alternatively, for RT-PCR analysis, total RNA was prepared from the excised tissues using the RNeasy Mini Kit (Qiagen).

Western Blotting

Anti-Derlin-3 antibody was raised in rabbits against a keyhole limpet hemocyanin–conjugated peptide, D^{215}PDYLPLPEEQPEL^{228}, derived from mouse Derlin-3. Anti-Herp was raised against S^{122}DGLRQREVLRNLS^{135}, derived from mouse Herp. These antibodies were subjected to affinity purification before use. Anti-Derlin-1 (MBL), anti-Derlin-2 (MBL), anti-HRD1 (Abgent), anti-VIMP (Sigma), anti-p97 (Santa Cruz Biotechnology), anti-KDEL (Stressgen Biotechnologies), anti-ß-actin (Sigma), and anti-GFP (Clontech) antibodies were purchased for use. Tissue homogenates were subjected to SDS-PAGE and transferred to PVDF membranes (Bio-Rad). The membranes were blocked with 5% skim milk, incubated with primary antibodies, and then incubated with HRP-labeled anti-rabbit or mouse IgG (Kirkegaard & Perry Laboratories). Signals were developed using Immobilon Western Chemiluminescent HRP Substrate (Millipore), and detected using an Image Analyzer LAS-3000 (Fujifilm).

RT-PCR

Total RNA prepared from mouse tissues was subjected to RT-PCR using the OneStep RT-PCR Kit (Qiagen). The primer sequences and product sizes are listed in Table S1. RT-PCR for XBP1 was designed to amplify both 140-bp (unspliced form) and 114-bp (spliced form) products. The PCR products were separated by polyacrylamide gel electrophoresis and stained with SYBR Green I Nucleic Acid Gel Stain (Lonza). The bands were detected with the LAS-3000 and quantified using the Image Gauge software (Fujifilm). Band intensities were normalized against GAPDH for target genes other than XBP1. For XBP1, the ratios of the spliced form to the unspliced plus spliced forms were evaluated.

Hydrodynamics-Based *In Vivo* Gene Transfection

The open reading frame of NHK was inserted into pAcGFP1-N1 plasmid vector (Clontech) for expression of NHK-GFP. The plasmid DNA was injected into male mice using a hydrodynamics-based transfection technique [31]. Briefly, 5 μg of the plasmid DNA was diluted in 1.5–2.2 ml (a volume equivalent to 8% of the body weight) of TransIT-EE Delivery Solution (Mirus Bio) and injected via the tail vein within 5–10 s. After 12 h, the anesthetized mice were perfused with PBS, and their liver was excised. Alternatively, the proteasome inhibitor epoxomicin (Peptide Institute, 0.2 mM dissolved in PBS) were intraperitoneally injected into mice at a dose of 15 μl/g body weight 12 h after hydrodynamics-based transfection, and after 12 h, the liver was excised. The liver tissues were homogenized by Polytron PT1200 in an ice-cold buffer (10 mM HEPES, 220 mM mannitol, 70 mM sucrose; pH 7.4) containing Complete Protease Inhibitor Cocktail (Roche), and subjected to subcellular fractionation using centrifugation. The microsomes were solubilized by a buffer containing 1% digitonin on ice, and subjected to Western blotting after removal of debris by centrifugation.

Glucose Tolerance and Insulin Response Tests

Glucose (200 mg/ml) was intraperitoneally injected into 13-week-old fasted male mice (2 mg/g body weight). Alternatively, human insulin (100 mU/ml, Lilly) was intraperitoneally injected into 14-week-old fasted male mice (1 mU/g body weight). Before the injection and 15, 30, 60, and 120 min postinjection, a drop of blood was collected from the tail end, and the glucose level was measured using GlucoCard GT-1810 (Arkray). All mice examined were confirmed to carry the normal *Nnt* (nicotinamide nucleotide transhydrogenase) gene by PCR-based genotyping using primer pairs, CAGGTAAGAAAGCTCCTGTTT/GTGCATTGAACCCTCAAAGG for the normal allele product (235 bp) and GTCTGATACGTCCTTCATGGT/CTAGCCTTTCAGTTTTCAGGA for the deleted allele product (344 bp). *Nnt* is occasionally disrupted by deletion of exons 7–11 in the C57BL/6J

mouse substrains, which may lead to glucose intolerance and reduced insulin secretion [43,44].

Ischemia Stroke Model

To assess tolerance to cerebral ischemia, 9-week-old male mice were subjected to the three-vessel occlusion technique [45,46]. Briefly, the bilateral common carotid arteries were exposed and clipped under anesthesia to cause occlusion for the desired period of time. The left middle cerebral artery (MCA) was exposed by drilling a burr hole in the skull, and cauterized at the lateral edge of the olfactory tract to induce focal ischemia for cortical neurons in the MCA region. After 30 min of the three-vessel occlusion, the clips on the common carotid arteries were removed, which effectively terminate the induction of focal ischemia by increasing the collateral cerebral blood flow toward the targeted MCA territory up to the level that normal neurons never die. After 24 h, the mice were administered an overdose of pentobarbital and intracardially perfused with ice-cold PBS. The brain was removed, cut into six 1-mm-thick slices beginning at the frontal tip, and immersed in 2% 2,3,5-triphenyl-tetrazolium chloride to stain the viable tissues. The slices were then immersed in 4% paraformaldehyde/PBS, and the infarct lesion and hemispheric areas of each slice were measured by computer-assisted image analysis system. Finally, the infarct lesion size was adjusted for edema (infarction index) and calculated for each animal.

Supporting Information

Figure S1 Expression of Derlin-1 in *Derl1*$^{+/+}$, *Derl1*$^{+/-}$, and *Derl1*$^{-/-}$ mouse embryos. The embryos resulting from *Derl1*$^{+/-}$ matings were isolated from uteri at E7.5. Approximately half of each embryo was used for DNA preparation followed by PCR-genotyping, and the other half was subjected to Western blotting using anti-Derlin-1 and anti-ß-actin antibodies.
(PDF)

Figure S2 Western blotting analysis of liver, pancreas, and kidneys from wild-type (WT), *Derl3*$^{-/-}$, and *Herpud1*$^{-/-}$ mice. Mice were intraperitoneally injected with PBS as control (C) or tunicamycin (Tm) 12 h before sacrifice. Liver, pancreas, and kidney homogenates were subjected to Western blotting using the indicated antibodies. Band intensities were normalized to the mean intensity of PBS-injected WT mice (for samples other than Derlin-3 and Herp) or Tm-injected WT mice (for Derlin-3 and Herp). Data are expressed as means with range ($n = 2$). The original blots are shown in Figure 3.
(PDF)

Table S1 Primer sequences for genotyping PCR and RT-PCR.
(PDF)

Author Contributions

Conceived and designed the experiments: YE TM KK. Performed the experiments: YE HY YA TO KK. Analyzed the data: YE HY TM KK. Wrote the paper: YE TM KK.

References

1. Tsai B, Ye Y, Rapoport TA (2002) Retro-translocation of proteins from the endoplasmic reticulum into the cytosol. Nat Rev Mol Cell Biol 3: 246–255.
2. Meusser B, Hirsch C, Jarosch E, Sommer T (2005) ERAD: the long road to destruction. Nat Cell Biol 7: 766–772.
3. Vembar SS, Brodsky JL (2008) One step at a time: endoplasmic reticulum-associated degradation. Nat Rev Mol Cell Biol 9: 944–957.
4. Hirsch C, Gauss R, Horn SC, Neuber O, Sommer T (2009) The ubiquitylation machinery of the endoplasmic reticulum. Nature 458: 453–460.
5. Hampton RY, Gardner RG, Rine J (1996) Role of 26S proteasome and HRD genes in the degradation of 3-hydroxy-3-methylglutaryl-CoA reductase, an integral endoplasmic reticulum membrane protein. Mol Biol Cell 7: 2029–2044.
6. Bordallo J, Plemper RK, Finger A, Wolf DH (1998) Der3p/Hrd1p is required for endoplasmic reticulum-associated degradation of misfolded lumenal and integral membrane proteins. Mol Biol Cell 9: 209–222.
7. Carvalho P, Stanley AM, Rapoport TA (2010) Retrotranslocation of a misfolded luminal ER protein by the ubiquitin-ligase Hrd1p. Cell 143: 579–591.
8. Lilley BN, Ploegh HL (2005) Multiprotein complexes that link dislocation, ubiquitination, and extraction of misfolded proteins from the endoplasmic reticulum membrane. Proc Natl Acad Sci USA 102: 14296–14301.
9. Schulze A, Standera S, Buerger E, Kikkert M, van Voorden S, et al. (2005) The ubiquitin-domain protein HERP forms a complex with components of the endoplasmic reticulum associated degradation pathway. J Mol Biol 354: 1021–1027.
10. Kny M, Standera S, Hartmann-Petersen R, Kloetzel PM, Seeger M (2011) Herp regulates Hrd1-mediated ubiquitylation in a ubiquitin-like domain-dependent manner. J Biol Chem 286: 5151–5156.
11. Knop M, Finger A, Braun T, Hellmuth K, Wolf DH (1996) Der1, a novel protein specifically required for endoplasmic reticulum degradation in yeast. EMBO J 15: 753–763.
12. Lilley BN, Ploegh HL (2004) A membrane protein required for dislocation of misfolded proteins from the ER. Nature 429: 834–840.
13. Oda Y, Okada T, Yoshida H, Kaufman RJ, Nagata K, et al. (2006) Derlin-2 and Derlin-3 are regulated by the mammalian unfolded protein response and are required for ER-associated degradation. J Cell Biol 172: 383–393.
14. Ye Y, Shibata Y, Yun C, Ron D, Rapoport TA (2004) A membrane protein complex mediates retro-translocation from the ER lumen into the cytosol. Nature 429: 841–847.
15. Wahlman J, DeMartino GN, Skach WR, Bulleid NJ, Brodsky JL, et al. (2007) Real-time fluorescence detection of ERAD substrate retrotranslocation in a mammalian in vitro system. Cell 129: 943–955.
16. Kokame K, Agarwala KL, Kato H, Miyata T (2000) Herp, a new ubiquitin-like membrane protein induced by endoplasmic reticulum stress. J Biol Chem 275: 32846–32853.
17. Kokame K, Kato H, Miyata T (2001) Identification of ERSE-II, a new cis-acting element responsible for the ATF6-dependent mammalian unfolded protein response. J Biol Chem 276: 9199–9205.
18. Sai X, Kawamura Y, Kokame K, Yamaguchi H, Shiraishi H, et al. (2002) Endoplasmic reticulum stress-inducible protein, Herp, enhances presenilin-mediated generation of amyloid ß-protein. J Biol Chem 277: 12915–12920.
19. Sai X, Kokame K, Shiraishi H, Kawamura Y, Miyata T, et al. (2003) The ubiquitin-like domain of Herp is involved in Herp degradation, but not necessary for its enhancement of amyloid ß-protein generation. FEBS Lett 553: 151–156.
20. Hori O, Ichinoda F, Yamaguchi A, Tamatani T, Taniguchi M, et al. (2004) Role of Herp in the endoplasmic reticulum stress response. Genes Cells 9: 457–469.
21. Chan SL, Fu W, Zhang P, Cheng A, Lee J, et al. (2004) Herp stabilizes neuronal Ca^{2+} homeostasis and mitochondrial function during endoplasmic reticulum stress. J Biol Chem 279: 28733–28743.
22. Chigurupati S, Wei Z, Belal C, Vandermey M, Kyriazis GA, et al. (2009) The homocysteine-inducible endoplasmic reticulum stress protein counteracts calcium store depletion and induction of CCAAT enhancer-binding protein homologous protein in a neurotoxin model of Parkinson disease. J Biol Chem 284: 18323–18333.
23. Kim TY, Kim E, Yoon SK, Yoon JB (2008) Herp enhances ER-associated protein degradation by recruiting ubiquilins. Biochem Biophys Res Commun 369: 741–746.
24. Okuda-Shimizu Y, Hendershot LM (2007) Characterization of an ERAD pathway for nonglycosylated BiP substrates, which require Herp. Mol Cell 28: 544–554.
25. Liang G, Li Q, Tang Y, Kokame K, Kikuchi T, et al. (2008) Polycystin-2 is regulated by endoplasmic reticulum-associated degradation. Hum Mol Genet 17: 1109–1119.
26. Horn SC, Hanna J, Hirsch C, Volkwein C, Schutz A, et al. (2009) Usa1 functions as a scaffold of the HRD-ubiquitin ligase. Mol Cell 36: 782–793.
27. Carroll SM, Hampton RY (2010) Usa1p is required for optimal function and regulation of the Hrd1p endoplasmic reticulum-associated degradation ubiquitin ligase. J Biol Chem 285: 5146–5156.
28. Yagishita N, Ohneda K, Amano T, Yamasaki S, Sugiura A, et al. (2005) Essential role of synoviolin in embryogenesis. J Biol Chem 280: 7909–7916.
29. Dougan SK, Hu CC, Paquet ME, Greenblatt MB, Kim J, et al. (2011) Derlin-2-deficient mice reveal an essential role for protein dislocation in chondrocytes. Mol Cell Biol 31: 1145–1159.
30. Yoshida H, Matsui T, Yamamoto A, Okada T, Mori K (2001) XBP1 mRNA is induced by ATF6 and spliced by IRE1 in response to ER stress to produce a highly active transcription factor. Cell 107: 881–891.

31. Liu F, Song Y, Liu D (1999) Hydrodynamics-based transfection in animals by systemic administration of plasmid DNA. Gene Ther 6: 1258–1266.
32. Hosokawa N, Tremblay LO, You Z, Herscovics A, Wada I, et al. (2003) Enhancement of endoplasmic reticulum (ER) degradation of misfolded Null Hong Kong α1-antitrypsin by human ER mannosidase I. J Biol Chem 278: 26287–26294.
33. Greenblatt EJ, Olzmann JA, Kopito RR (2011) Derlin-1 is a rhomboid pseudoprotease required for the dislocation of mutant α-1 antitrypsin from the endoplasmic reticulum. Nat Struct Mol Biol 18: 1147–1152.
34. Hosokawa N, Wada I, Nagasawa K, Moriyama T, Okawa K, et al. (2008) Human XTP3-B forms an endoplasmic reticulum quality control scaffold with the HRD1-SEL1L ubiquitin ligase complex and BiP. J Biol Chem 283: 20914–20924.
35. Francisco AB, Singh R, Li S, Vani AK, Yang L, et al. (2010) Deficiency of suppressor enhancer Lin12 1 like (SEL1L) in mice leads to systemic endoplasmic reticulum stress and embryonic lethality. J Biol Chem 285: 13694–13703.
36. Christianson JC, Olzmann JA, Shaler TA, Sowa ME, Bennett EJ, et al. (2012) Defining human ERAD networks through an integrative mapping strategy. Nat Cell Biol 14: 93–105.
37. Marciniak SJ, Ron D (2006) Endoplasmic reticulum stress signaling in disease. Physiol Rev 86: 1133–1149.
38. Scheuner D, Kaufman RJ (2008) The unfolded protein response: a pathway that links insulin demand with ß-cell failure and diabetes. Endocr Rev 29: 317–333.
39. Harding HP, Zeng H, Zhang Y, Jungries R, Chung P, et al. (2001) Diabetes mellitus and exocrine pancreatic dysfunction in perk−/− mice reveals a role for translational control in secretory cell survival. Mol Cell 7: 1153–1163.
40. Iwawaki T, Akai R, Kohno K (2010) IRE1α disruption causes histological abnormality of exocrine tissues, increase of blood glucose level, and decrease of serum immunoglobulin level. PLoS One 5: e13052.
41. DeGracia DJ, Montie HL (2004) Cerebral ischemia and the unfolded protein response. J Neurochem 91: 1–8.
42. Ogawa S, Kitao Y, Hori O (2007) Ischemia-induced neuronal cell death and stress response. Antioxid Redox Signal 9: 573–587.
43. Toye AA, Lippiat JD, Proks P, Shimomura K, Bentley L, et al. (2005) A genetic and physiological study of impaired glucose homeostasis control in C57BL/6J mice. Diabetologia 48: 675–686.
44. Freeman H, Shimomura K, Horner E, Cox RD, Ashcroft FM (2006) Nicotinamide nucleotide transhydrogenase: a key role in insulin secretion. Cell Metab 3: 35–45.
45. Yanamoto H, Xue JH, Miyamoto S, Nagata I, Nakano Y, et al. (2004) Spreading depression induces long-lasting brain protection against infarcted lesion development via BDNF gene-dependent mechanism. Brain Res 1019: 178–188.
46. Yamamoto H, Kokame K, Okuda T, Nakajo Y, Yanamoto H, et al. (2011) NDRG4 protein-deficient mice exhibit spatial learning deficits and vulnerabilities to cerebral ischemia. J Biol Chem 286: 26158–26165.

References

1 Oyelese Y, Ananth CV. Postpartum hemorrhage: epidemiology, risk factors, and causes. *Clin Obstet Gynecol* 2010; **53**: 147–56.
2 Biguzzi E, Franchi F, Ambrogi F, Ibrahim B, Bucciarelli P, Acaia B, Radaelli T, Biganzoli E, Mannucci PM. Risk factors for postpartum hemorrhage in a cohort of 6011 Italian women. *Thromb Res* 2012; **129**: e1–7.
3 Peyvandi F, Garagiola I, Menegatti M. Gynecological and obstetrical manifestations of inherited bleeding disorders in women. *J Thromb Haemost* 2011; **9**(Suppl. 1): 236–45.
4 Charbit B, Mandelbrot L, Samain E, Baron G, Haddaoui B, Keita H, Sibony O, Mahieu-Caputo D, Hurtaud-Roux MF, Huisse MG, Denninger MH, de Prost D. The decrease of fibrinogen is an early predictor of the severity of postpartum hemorrhage. *J Thromb Haemost* 2007; **5**: 266–73.
5 Fawcus S. Treatments for primary postpartum haemorrhage: RHL commentary (last revised: 8 May 2007). *The WHO Reproductive Health Library*, Geneva: World Health Organization. Available from: http://apps.who.int/rhl/pregnancy_childbirth/childbirth/postpartum_haemorrhage/sfcom/en/index.html (accessed 14th April 2011).
6 Simon L, Santi TM, Sacquin P, Hamza J. Pre-anaesthetic assessment of coagulation abnormalities in obstetric patients: usefulness, timing and clinical implications. *Br J Anaesth* 1997; **78**: 678–83.

Large infarct and high mortality by cerebral ischemia in mice carrying the factor V Leiden mutation

T. KITA,* F. BANNO,* H. YANAMOTO,†‡ Y. NAKAJO,† K. IIHARA‡ and T. MIYATA*

**Department of Molecular Pathogenesis, National Cerebral and Cardiovascular Center, Suita, Osaka; †Laboratory of Neurology and Neurosurgery, National Cerebral and Cardiovascular Center, Suita, Osaka; and ‡Department of Cerebrovascular Surgery, National Cerebral and Cardiovascular Center, Suita, Osaka, Japan*

To cite this article: Kita T, Banno F, Yanamoto H, Nakajo Y, Iihara K, Miyata T. Large infarct and high mortality by cerebral ischemia in mice carrying the factor V Leiden mutation. *J Thromb Haemost* 2012; **10:** 1453–5.

Factor V Leiden (FVL) mutation (R506Q mutation) is an established risk factor for venous thromboembolism due to a hypercoagulable state through the resistance to activated protein C [1]. The FVL mutation also exerts a modest effect on arterial ischemic diseases. It is associated with ischemic stroke in children [2] and in young adults [3] and appears to be weakly associated with ischemic stroke in the general adult population [4]. A mouse model carrying a targeted homologous mutation at R504 to Q in FV has been developed [5] and studied under various stimulations or pathophysiologic conditions [6–8]. However, the role of the FVL mutation in ischemic stroke has not been confirmed using the mouse model. In this study, we applied brain ischemia-reperfusion injury in FVL mice using the three-vessel occlusion technique [9]. This technique produces a constant infarcted lesion limited to within the neocortex with small variances and does not require intraluminal thread insertion, which might activate the coagulation system during ischemia.

Correspondence: Toshiyuki Miyata, Department of Molecular Pathogenesis, National Cerebral and Cardiovascular Center, 5-7-1 Fujishirodai, Suita, Osaka 565-8565, Japan.
Tel.: +81 6 6833 5012; fax: +81 6 6835 1176.
E-mail: miyata@ri.ncvc.go.jp

DOI: 10.1111/j.1538-7836.2012.04776.x

Received 15 April 2012, accepted 25 April 2012

Male young adult mice (7–18 weeks old) of wild-type $Fv^{+/+}$, heterozygous $Fv^{Q/+}$ and homozygous $Fv^{Q/Q}$ (Jackson Labs, Bar Harbor, ME, USA) were used for the experiments. All animal procedures were approved by the Animal Care and Use Committees of the National Cerebral and Cardiovascular Center. Temporary focal ischemia was induced using the three-vessel occlusion technique as described previously [9]. Briefly, we electrocauterized the distal M1 portion of the left middle cerebral artery, peripheral to the perforating arteries of the basal ganglia, and made temporal occlusions on the bilateral common carotid arteries for 15 min using vascular clips. After 24 h, neurological deficits were assessed using a scoring scale (from 0 to 4) as described [10,11], and the brains were excised and stained with 2, 3, 5-triphenyl tetrazolium chloride. The infarct and total hemispheric volumes were measured as described [10]. The infarct volume was adjusted for edema by dividing the volume by the edema index (left hemisphere volume/right hemisphere volume) [10,11]. The regional cerebral blood flow (rCBF) at the penumbra-like area of the left hemisphere was monitored using a laser-Doppler blood flowmeter TBF-LN1 (Unique Medical, Tokyo, Japan) [9,10]. In separate experimental groups the survival of the mice was monitored for 7 days after ischemia and graphed using a Kaplan–Meyer plot. Data were analyzed by the one-way ANOVA test followed by the post hoc Bonferroni's multiple comparison test. Survival rates were analyzed by the Mantel-Cox log-rank test. Data were expressed as the means ± standard deviation. P-values < 0.05 were considered significant.

Infarct volumes 24 h after ischemia in $Fv^{Q/+}$ and $Fv^{Q/Q}$ mice were significantly larger than those in $Fv^{+/+}$ mice (15.9 ± 5.3 mm^3 in $Fv^{+/+}$, n = 11; 26.7 ± 4.8 mm^3 in $Fv^{Q/+}$, n = 12; 29.9 ± 4.1 mm^3 in $Fv^{Q/Q}$ mice, n = 8; $Fv^{+/+}$ vs. $Fv^{Q/+}$, $P < 0.001$; $Fv^{+/+}$ vs. $Fv^{Q/Q}$, $P < 0.001$) (Fig. 1A,B). The edema index (1.06 ± 0.03 in $Fv^{+/+}$, 1.05 ± 0.02 in $Fv^{Q/+}$, 1.04 ± 0.04 in $Fv^{Q/Q}$) and the neurological deficit score (2.82 ± 0.40 in $Fv^{+/+}$, 2.58 ± 0.67 in $Fv^{Q/+}$, 2.75 ± 0.46 in $Fv^{Q/Q}$) were not different among the groups. The rCBF during ischemia in $Fv^{Q/Q}$ mice (9.9 ± 1.2%, n = 7) was more severely decreased than in either $Fv^{+/+}$ (21.2 ± 0.5%, n = 7) or $Fv^{Q/+}$ mice (19.5 ± 2.0%, n = 7) ($P < 0.001$) (Fig. 1C). In every group, the rCBF was recovered to the preischemic normal level immediately after removal of the vascular clips, ensuring sufficient reperfusion of the left middle cerebral artery territory. $Fv^{Q/Q}$ mice started to die from day 2, and only two out of seven mice survived for 7 days (Fig. 1D). $Fv^{Q/+}$ mice started to die from day 4, and only two mice survived. Two $Fv^{+/+}$ mice died on day 7, and the remaining five survived. The 7-day survival in $Fv^{Q/+}$ and $Fv^{Q/Q}$ mice was significantly lower than that in $Fv^{+/+}$ mice ($P < 0.05$).

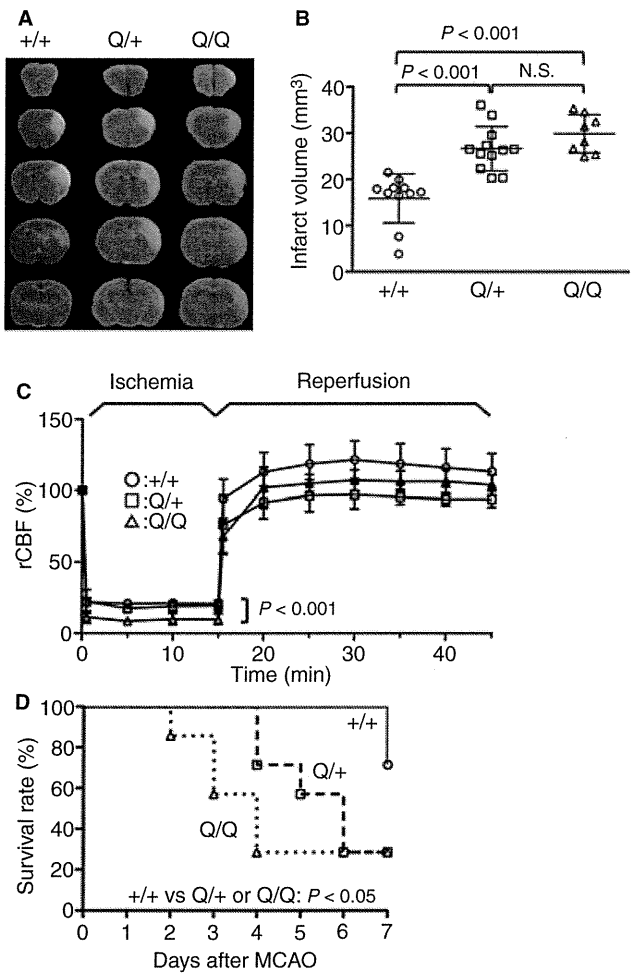

Fig. 1. Effects of factor V Leiden (FVL) on focal ischemia. (A) Representative images of coronal sections of $Fv^{+/+}$, $Fv^{Q/+}$ and $Fv^{Q/Q}$ mouse brains. *Red* areas represent vital brain tissue and *white* areas represent cerebral infarction. (B) Infarct volumes of $Fv^{+/+}$ (○), $Fv^{Q/+}$ (□) and $Fv^{Q/Q}$ (△) mice. *Bars* represent the means ± standard deviation. N.S., not significantly different ($P > 0.05$). (C) rCBF of $Fv^{+/+}$, $Fv^{Q/+}$ and $Fv^{Q/Q}$ mice during 15-min ischemia and 30-min reperfusion. The rCBFs were expressed as percentages of the baseline flow obtained before middle cerebral artery occlusion. Data are the means ± standard deviation of seven mice per group. (D) Seven-day survival of $Fv^{+/+}$, $Fv^{Q/+}$ and $Fv^{Q/Q}$ mice after temporary ischemia (n = 7/group).

We demonstrated that both $Fv^{Q/+}$ and $Fv^{Q/Q}$ mice showed increased infarct volumes and decreased long-term survival compared with $Fv^{+/+}$ mice after the temporary focal ischemia-reperfusion stress. Although the three-vessel occlusion technique does not activate the coagulation system during ischemia, the infarct lesion was larger in $Fv^{Q/+}$ or $Fv^{Q/Q}$ mice than in $Fv^{+/+}$ mice. The reperfusion process after transient cerebral ischemia is known to induce many cellular events, including the loss of normal permeability in the blood brain barrier, which deteriorates cerebral metabolism, increases cerebral damage [12], and induces ischemic cerebral damage-related secondary activation of the coagulation system with subsequent thrombus formation around the infarct lesion [13]. The hypercoagulable state of FVL, which can enhance reperfusion injury after ischemia, is considered to be the primary cause of both the enlargement of infarct lesions and the vulnerability of the brain after ischemic stroke. The other possible pathophysiology is that FVL may have affected some of the intrinsic vascular and/or neuronal protection systems.

The findings that both $Fv^{Q/+}$ and $Fv^{Q/Q}$ mice showed larger infarct volumes and lower survival rates than $Fv^{+/+}$ mice after temporary focal ischemia-reperfusion stress support a direct causal relationship between the FVL mutation and increased susceptibility to ischemic stroke in young adult individuals.

Acknowledgements

This work was supported by grants-in-aid from the Ministry of Health, Labour and Welfare of Japan, the Ministry of Education, Culture, Sports, Science and Technology of Japan,; the Program for the Promotion of Fundamental Studies in Health Sciences of the National Institute of Biomedical Innovation (NIBIO) of Japan, and the Mitsubishi Pharma Research Foundation.

Disclosure of Conflict of Interests

The authors state that they have no conflict of interest.

References

1 Svensson PJ, Dahlback B. Resistance to activated protein C as a basis for venous thrombosis. *N Engl J Med* 1994; **330**: 517–22.
2 Kenet G, Sadetzki S, Murad H, Martinowitz U, Rosenberg N, Gitel S, Rechavi G, Inbal A. Factor V Leiden and antiphospholipid antibodies are significant risk factors for ischemic stroke in children. *Stroke* 2000; **31**: 1283–8.
3 Hamedani AG, Cole JW, Mitchell BD, Kittner SJ. Meta-analysis of factor V Leiden and ischemic stroke in young adults: the importance of case ascertainment. *Stroke* 2010; **41**: 1599–603.
4 Casas JP, Hingorani AD, Bautista LE, Sharma P. Meta-analysis of genetic studies in ischemic stroke: thirty-two genes involving approximately 18, cases and 58,000 controls. *Arch Neurol* 2004; **61**: 1652–61.

5 Cui J, Eitzman DT, Westrick RJ, Christie PD, Xu ZJ, Yang AY, Purkayastha AA, Yang TL, Metz AL, Gallagher KP, Tyson JA, Rosenberg RD, Ginsburg D. Spontaneous thrombosis in mice carrying the factor V Leiden mutation. *Blood* 2000; **96**: 4222–6.
6 Eitzman DT, Westrick RJ, Shen Y, Bodary PF, Gu S, Manning SL, Dobies SL, Ginsburg D. Homozygosity for factor V Leiden leads to enhanced thrombosis and atherosclerosis in mice. *Circulation* 2005; **111**: 1822–5.
7 Nagai N, Lijnen HR, Cleuren AC, Rosendaal FR, van Hoef B, Hoylaerts MF, van Vlijmen BJ. Factor V Leiden mutation is associated with enhanced arterial thrombotic tendency in lean but not in obese mice. *Thromb Haemost* 2007; **98**: 858–63.
8 Cooley BC, Chen CY, Schmeling G. Increased venous versus arterial thrombosis in the Factor V Leiden mouse. *Thromb Res* 2007; **119**: 747–51.
9 Yanamoto H, Nagata I, Niitsu Y, Xue JH, Zhang Z, Kikuchi H. Evaluation of MCAO stroke models in normotensive rats: standardized neocortical infarction by the 3VO technique. *Exp Neurol* 2003; **182**: 261–74.
10 Yamamoto H, Kokame K, Okuda T, Nakajo Y, Yanamoto H, Miyata T. NDRG4 protein-deficient mice exhibit spatial learning deficits and vulnerabilities to cerebral ischemia. *J Biol Chem* 2011; **286**: 26158–65.
11 Yanamoto H, Nagata I, Niitsu Y, Zhang Z, Xue JH, Sakai N, Kikuchi H. Prolonged mild hypothermia therapy protects the brain against permanent focal ischemia. *Stroke* 2001; **32**: 232–9.
12 Nabavi DG, Droste DW, Kemeny V, Schulte-Altedorneburg G, Weber S, Ringelstein EB. Potential and limitations of echocontrast-enhanced ultrasonography in acute stroke patients: a pilot study. *Stroke* 1998; **29**: 949–54.
13 Iba T, Kidokoro A, Fukunaga M, Takuhiro K, Ouchi M, Ito Y. Comparison of the protective effects of type III phosphodiesterase (PDE3) inhibitor (cilostazol) and acetylsalicylic acid on intestinal microcirculation after ischemia reperfusion injury in mice. *Shock* 2006; **26**: 522–6.

Different bleeding risk in type 2A and 2M von Willebrand disease: a 2-year prospective study in 107 patients: a rebuttal

E. J. FAVALORO,* R. BONAR† and K. MARSDEN†
**Haematology, Institute of Clinical Pathology and Medical Research (ICPMR), Westmead Hospital, Westmead, NSW; and †Royal College of Pathology of Australasia (RCPA) Haematology Quality Assurance Program (QAP), Northmead, NSW, Australia*

To cite this article: Favaloro EJ, Bonar R, Marsden K. Different bleeding risk in type 2A and 2M von Willebrand disease: a 2-year prospective study in 107 patients: a rebuttal. *J Thromb Haemost* 2012; **10:** 1455–8.

See also Castaman G, Baronciani L, Canciani MT, Federici AB. Different bleeding risk in type 2A and 2M von Willebrand disease: a 2-year prospective study in 107 patients: a reply to a rebuttal. This issue, pp 1458–60.

We were very interested to read the recent report by Castaman *et al.* [1] in this journal. This study described an increased bleeding risk in patients with type 2A von Willebrand disease (VWD) as compared with those with type 2M VWD. This is an important finding, and should provide support for the ongoing diagnostic differentiation of type 2A and type 2M VWD. The exact frequencies of these two forms of VWD are unknown, although a recent geographically global analysis indicated much variability in their perceived incidence [2], with type 2A and type 2M VWD, respectively, reported as comprising 5.5–82.6% and 0–56.3% (Fig. 1A) of all cases of type 2 VWD. Interestingly, there was a strong negative correlation between their relative 'incidence' (see Fig. 1B), such that laboratories identifying more cases of type 2A VWD reported fewer cases of type 2M VWD, and vice versa. However, most centers reported far more cases of type 2A VWD than of type 2M VWD, and only a few centers identified type 2M VWD as comprising a high proportion of type 2 VWD cases. These data do not reflect a variation in the frequencies of type 2A and type 2M VWD according to geography, but rather a differential ability of laboratories to appropriately identify type 2M VWD, as well as diagnostic biases related to perceptions of VWD classification. Indeed, as reported by Castaman *et al.* [1], 'VWD2M is often difficult to diagnose accurately because of its phenotype which can be difficult to differentiate from VWD1 or VWD2A unless a full range of phenotypic evaluations is carried out'. According to our regional external quality assurance (EQA) experience, type 2M VWD is typically misidentified as type 1 or type 2A VWD, because of laboratories either using only limited von Willebrand factor (VWF) test panels or misinterpreting their own test data [3].

According to the latest ISTH VWF Scientific Standardization Committee (SSC) classification, as used by Castaman *et al.* [1], type 2A reflects 'decreased VWF-dependent platelet

Correspondence: Emmanuel J. Favaloro, Department of Haematology, Institute of Clinical Pathology and Medical Research (ICPMR), Westmead Hospital, Westmead, NSW 2145, Australia.
Tel.: +612 9845 6618; fax: +612 9689 2331.
E-mail: emmanuel.favaloro@swahs.health.nsw.gov.au

DOI: 10.1111/j.1538-7836.2012.04781.x

Received 17 April 2012, accepted 9 May 2012

J. Biochem. 2012;152(3):251–258 doi:10.1093/jb/mvs066

JB THE JOURNAL OF BIOCHEMISTRY

Binding of von Willebrand factor cleaving protease ADAMTS13 to Lys-plasmin(ogen)

Received February 2, 2012; accepted May 13, 2012; published online June 7, 2012

Yongchol Shin[1,2,*], Masashi Akiyama[1], Koichi Kokame[1], Kenji Soejima[3] and Toshiyuki Miyata[1,†]

[1]Department of Molecular Pathogenesis, National Cerebral and Cardiovascular Center, Suita, 5-7-1 Fujishirodai, Suita, Osaka 5658565, Japan; [2]Department of Applied Chemistry, Kogakuin University, 2665-1 Nakano-cho, Hachioji, Tokyo 1920015, Japan; and [3]Research Department 1, Chemo-Sero-Therapeutic Research Institute, 1314-1 Kawabe, Kyokushi, Kikuchi, Kumamoto 8691298, Japan

*Yongchol Shin, Department of Applied Chemistry, Kogakuin University, 2665-1 Nakano-cho, Hachioji, Tokyo 1920015, Japan. Tel: +81-42-673-1491, email: shin@cc.kogakuin.ac.jp

†Toshiyuki Miyata, Department of Molecular Pathogenesis, National Cerebral and Cardiovascular Center, 5-7-1 Fujishirodai, Suita, Osaka 5658565, Japan. Tel: +81-6-6833-5012 ext. 2512, Fax: +81-6-6835-1176, email: miyata@ri.ncvc.go.jp

The metalloprotease ADAMTS13 affects platelet adhesion and aggregation through depolymerization of von Willebrand factor (VWF) multimers. Identification of ADAMTS13-binding proteins would reveal the hitherto unrecognized mechanisms underlying microvascular thrombus. To identify ADAMTS13-binding proteins, we performed a yeast two-hybrid screen using the Cys-rich and spacer domains of ADAMTS13, the critical regions for the binding and cleavage of VWF, as a bait region. We identified Lys-plasminogen, an amino-terminal truncated form of plasminogen, as the binding protein to ADAMTS13. Intact Glu-plasminogen did not bind to ADAMTS13. Active-site blocked Lys-plasmin bound to ADAMTS13. Domain truncation of ADAMTS13 and elastase digest of plasminogen indicated that the Cys-rich and spacer domains of ADAMTS13 and the kringle 5 and protease domains of plasminogen served as the main binding sites. Biacore measurements revealed that Lys-plasminogen bound to ADAMTS13 with a K_d of $1.9 \pm 0.1 \times 10^{-7}$ M and Glu-plasminogen exhibited a significantly lower affinity to ADAMTS13. Specific activity measurements revealed that ADAMTS13 and Lys-plasmin were still active even after the binary complex was formed. The binding of ADAMTS13 to Lys-plasminogen may play an important role to localize these two proteases at sites of thrombus formation or vascular injury where the fibrinolytic system is activated.

Keywords: ADAMTS13/fibrinolysis/plasminogen/thrombotic thrombocytopenic purpura/von Willebrand factor.

Abbreviations: ADAMTS13, a disintegrin-like and metalloproteinase with thrombospondin type-1 motifs 13; APMSF, *p*-amidinophenyl methanesulfonyl fluoride; CUB, complement components C1r and C1s/urinary epidermal growth factor/bone morphogenic protein-1; Glu-Pg, Glu-plasminogen; HRP, horseradish peroxidase; Lys-Pg, Lys-plasminogen; mAb, monoclonal antibody; mini-Pg, mini-plasminogen; VWF, von Willebrand factor.

Platelet thrombus formation is dependent on the multimeric sizes of von Willebrand factor (VWF) under shear stress conditions. VWF multimers are depolymerized by plasma metalloprotease ADAMTS13. Thus, ADAMTS13 regulates the VWF-dependent platelet thrombus formation. Congenital or acquired deficiency of ADAMTS13 can cause thrombotic thrombocytopenic purpura that is characterized with thrombocytopoenia and microangiopathic haemolytic anaemia, sometimes accompanied with transient neurological dysfunction (*1–4*). ADAMTS13 has multiple discrete domains, comprising a metalloprotease domain (M), a disintegrin-like domain (D), a first thrombospondin type-1 repeat (T), a Cys-rich region (C), a spacer domain (S), seven consecutive T repeats and two CUB (Complement components C1r and C1s/urinary epidermal growth factor/bone morphogenic protein-1) domains (*5–7*).

ADAMTS13 cleaves a single specific peptide bond of Tyr^{1605}–Met^{1606} within the A2 domain of VWF under shear stress conditions *in vivo* or under denatured conditions *in vitro*. This restricted substrate specificity can be defined by several structural features in ADAMTS13. The C and S domains in ADAMTS13 play a critical role on the binding and cleavage of VWF, and the S domain seems to be highly important for the recognition of VWF (*8,9*). Studies using ADAMTS13 mutants and VWF peptides indicated cooperative and modular interaction of discrete segments of VWF with ADAMTS13 (*10–13*). The crystal structures of the DTCS domains showed three VWF-binding exosites on the linearly aligned discontinuous surfaces of the D, C and S domains (*14,15*). Two C-terminal CUB domains are also important for regulation of VWF cleavage *in vitro* as well as *in vivo* (*16–20*). Thus, the interaction between ADAMTS13 and VWF has been intensively investigated; however, the binding proteins for ADAMTS13 are not well known.

Fibrinolytic system in blood is involved in dissolution of blood clots and maintains a patent vascular system. The key component of the fibrinolytic system is plasmin that degrades fibrin clots. Plasmin is

generated from the inactive proenzyme, plasminogen, by cleavage of the Arg561–Val562 peptide bond. Two distinct physiological plasminogen activators, tissue type- or urokinase type-plasminogen activator, convert plasminogen to active plasmin on the fibrin or cell surface. Native plasminogen has N-terminal glutamic acid, designated Glu-plasminogen (Glu-Pg). Lys-plasminogen (Lys-Pg), an amino-terminal truncated form of plasminogen, is formed by the release of a 76-amino acid pre-activation peptide from intact Glu-Pg by the action of plasmin. Because Lys-Pg shows a more open conformation than Glu-Pg, plasminogen activators preferentially cleave Lys-Pg than Glu-Pg. To inhibit the fibrinolytic system, a plasminogen activator inhibitor-1 or α_2-plasmin inhibitor forms an inactive complex with plasminogen activator or plasmin, respectively (*21*).

In the present study, we performed a yeast two-hybrid screen using the critical regions, the C and S domains, for the VWF binding as a bait. The co-immunoprecipitation analysis, the far-western blotting and the Biacore measurement indicated that Lys-Pg is the binding protein to ADAMTS13. ADAMTS13 and Lys-plasmin were active even after the binary complex was formed. The binding of ADAMTS13 to Lys-Pg may play an important role to localize these two proteases at sites of thrombus formation or vascular injury where the fibrinolytic system is activated.

Materials and Methods

Yeast two-hybrid screen

The Matchmaker Two-hybrid System 3 (Clontech, Palo Alto, CA, USA) was used according to the manufacturer's instructions. A fragment encoding the C and S domains of human ADAMTS13 (amino acids 440–685) was used as the bait. cDNA libraries (Clontech) constructed from human liver and brain mRNA (1.3×10^8 and 1.4×10^7 clones, respectively) were screened. Insert DNA of positive clones was sequenced, and the sequence homologies were searched by basic local alignment search tool (BLAST).

Binding of ADAMTS13 to immobilized candidate proteins

The binding of ADAMTS13 (3 μg/ml) to immobilized proteins (9 μg/ml) was examined using microtiter plates. Bound ADAMTS13 to immobilized proteins was detected using anti-ADAMTS13 monoclonal antibody (mAb) WH2-22-1A, which recognizes the disintegrin-like domain (*22*), and horseradish peroxidase (HRP)-conjugated anti-mouse IgG antibody. Bound HRP activity was detected at 450 nm with a reference wavelength of 650 nm using 3,3′,5,5′-tetramethylbenzidine substrate (KPL, Gaithrburg, MD, USA) and a Multiskan Ascent microplate reader (Thermo, Waltham, MA, USA).

Co-immunoprecipitation analysis of ADAMTS13 with Glu-Pg or Lys-Pg

Human ADAMTS13 with a FLAG tag (ADAMTS13-FLAG) and two mutants, MD-FLAG constituting the M and D domains with the FLAG tag and MDTCS-FLAG constituting the M, D, T, C and S domains with the FLAG tag, were expressed in the culture medium using HeLa cells, as previously described (*8*). Culture medium containing each of those recombinant proteins was incubated with intact Glu-Pg (Calbiochem, Madison, WI, USA) and/or Lys-Pg (Calbiochem) in Tris-buffered saline (TBS: 50 mM Tris, 100 mM NaCl, pH 7.5) and immunoprecipitated with anti-FLAG M2 mAb-immobilized gel (Sigma-Aldrich, St. Louis, MO, USA). After washing with TBS containing 0.5% Tween-20 (TBS-T), proteins were eluted by the FLAG peptide, and subjected to SDS–PAGE for western blotting using anti-FLAG M2 mAb (Sigma) or anti-Pg mAb MAB2596 (R&D Systems, Minneapolis, MN, USA). Alternatively, we used the anti-Pg mAb and protein G-agarose (Sigma) for the co-immunoprecipitation analysis of purified ADAMTS13 (*22*) with Glu-Pg, Lys-Pg or *p*-amidinophenyl methanesulfonyl fluoride (APMSF)-treated Lys-plasmin (Calbiochem). Bound proteins were eluted with 100 mM glycine-HCl, pH 2.5, and then subjected to SDS–PAGE for western blotting using anti-ADAMTS13 mAb WH10, which recognizes the fourth thrombospondin type-1 repeat (*22*) or anti-Pg mAb MAB2596. Immunoblots were probed with HRP-conjugated anti-mouse IgG antibody. Protein bands were visualized using Western Lightning Chemiluminescence Reagent Plus (Perkin-Elmer, Waltham, MA, USA) on an image analyser LAS3000 (Fujifilm, Tokyo, Japan).

Identification of ADAMTS13 binding region in Lys-Pg

Lys-Pg (0.1 mg) was digested with porcine pancreatic elastase (5 μg; Sigma). The resulting mini-plasminogen (mini-Pg), a functionally active zymogen containing the kringle 5 and protease domains, and fragments containing the kringle 1–4 domains were obtained in the unbound and bound fractions, respectively, using a lysine-Sepharose column (GE Healthcare, Little Chalfont, UK) (*23*). Proteins were subjected to SDS–PAGE for N-terminal sequence analysis and transferred onto polyvinylidene difluoride membranes for far-western blotting. Proteins on the membranes were incubated with ADAMTS13. Bound ADAMTS13 was detected with the HRP-conjugated anti-ADAMTS13 polyclonal antibody (*22*) prepared using Peroxidase Labeling Kit-NH_2 (Dojindo, Kumamoto, Japan) and visualized using Western Lightning Chemiluminescence Reagent Plus on the image analyzer LAS3000.

Lys-Pg binding to ADAMTS13 using Biacore

The binding of Glu-Pg or Lys-Pg to ADAMTS13 was examined using a Biacore 2000 (GE healthcare, Piscataway, NJ, USA). ADAMTS13 was immobilized on a CM5 sensor chip with an amino coupling kit (GE healthcare) according to manufacturer's instructions. Approximately 500–600 resonance units (RU) of ADAMTS13 were covalently attached onto the chip. Lys-Pg (0.05, 0.1, 0.2, 0.4 and 0.8 μM) or Glu-Pg (0.4, 0.8, 1.6 and 3.2 μM) in 50 mM Tris, 100 mM NaCl, pH 7.5, containing 0.005% Tween-20 and 5 mM $CaCl_2$ was injected over the ADAMTS13-immobilized sensor chip at a flow rate of 20 μl/min for 2 min.

The sensor chip was regenerated with 50 mM Tris, 1 M NaCl, pH 7.5, containing 0.005% Tween-20 and 5 mM $CaCl_2$ for 1 min. The dissociation constants (K_d) at the equilibrium were obtained using several ligand concentrations with the BIA evaluation software. Each K_d value was obtained from four or three independent experiments using Lys-Pg or Glu-Pg, respectively.

Activity measurements of ADAMTS13 and plasmin in the complex

ADAMTS13 activity was measured using VWF (*24*) and synthetic fluorogenic substrate FRETS-VWF73 (Peptide Institute, Osaka, Japan) (*25*). For VWF assay, ADAMTS13 (15 ng/ml) was mixed with Glu-Pg (0.1 mg/ml), Lys-Pg (0.1 mg/ml) or bovine serum albumin (0.1 mg/ml) and incubated with guanidine-pretreated VWF multimers (2 mg/ml) for 30, 60 or 120 min at 37°C (*24*). The cleaved fragment with a molecular weight of 200 kDa was assessed by western blotting using HRP-conjugated anti-human VWF polyclonal antibody (DAKO, Carpinteria, CA, USA). For FRETS-VWF73 assay, ADAMTS13 (6.6×10^{-1} nM) was mixed with Glu-Pg (11, 110, 1100 nM) or Lys-Pg (12, 120, 1200 nM). After addition of FRETS-VWF73 (2 μM) to the mixture, increase in fluorescence was measured using Mx3000P System (Stratagene, La Jolla, CA, USA) with 340-nm excitation and 450-nm emission (*25*). The reaction rate was calculated by linear regression analysis of fluorescence over time from 0 min to 10 min using the PRISM software (GraphPad Software, San Diego, CA, USA). The relative activities were estimated from the activity of ADAMTS13 without Glu-Pg or Lys-Pg. To assess the plasmin activity, plasmin (20 nM) was preincubated with ADAMTS13 (40, 80, 200 nM) for 30 min at room temperature followed by the addition of S-2251 (1 mM). Plasmin activity was recorded as a change in absorbance at 405 nm with a reference wavelength of 492 nm during 30 min using the Multiskan Ascent microplate reader.

Results

Yeast two-hybrid screen for ADAMTS13

A yeast two-hybrid screen enabled us to identify more than 500 positive clones. A BLAST search for the insert DNA sequences identified approximately 200 genes, and 36 genes were categorized as membrane or secretory proteins. For further analysis, among these candidate genes, we selected nine secretory proteins that were commercially available or generously donated: Glu-Pg, biglycan (bovine), collagen type I, collagen type III, decorin (bovine), fibrinogen, laminin, histidine-rich glycoprotein and zinc-α2-glycoprotein. We found that ADAMTS13 was bound to immobilized Glu-Pg but not to the others (Fig. 1). The positive clone of human Pg contained a 676-bp cDNA fragment encoding the C-terminal 150 amino acids (amino acid residues 661–810) of the protease domain. ADAMTS13 also bound to Lys-Pg, an amino-terminal truncated form of Glu-Pg (Fig. 1).

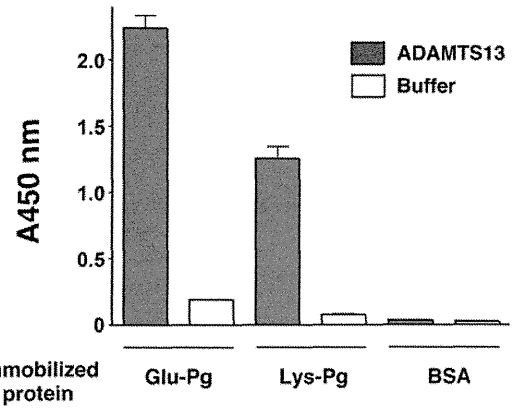

Fig. 1 Binding of ADAMTS13 to immobilized Glu-Pg and Lys-Pg. Microtitre wells were coated with Glu-Pg, Lys-Pg or BSA (each 9 μg/ml) and then incubated with or without ADAMTS13 (3 μg/ml). Bound ADAMTS13 was detected using anti-ADAMTS13 mAb WH2-22-1A (1 μg/ml) and HRP-conjugated anti-mouse IgG (0.25 μg/ml). After incubation with 3,3′,5,5′-tetramethylbenzidine substrate for 20 min, bound HRP activity was detected at 450 nm with a reference wavelength of 650 nm by a Multiskan Ascent microplate reader. The binding was expressed as the mean ± SD ($n = 3$). Grey bar, with ADAMTS13; white bar, without ADAMTS13.

ADAMTS13 binding to Pg

The binding of ADAMTS13 to Pg was examined by co-immunoprecipitation analysis. Anti-FLAG antibody immunoprecipitated ADAMTS13-FLAG with Lys-Pg but not with Glu-Pg (Fig. 2A). Next, anti-Pg antibody was used for the co-immunoprecipitation analysis. Again, ADAMTS13 was co-immunoprecipitated with only Lys-Pg but not with Glu-Pg (Fig. 2B). We found that APMSF-treated Lys-plasmin could be co-immunoprecipitated with ADAMTS13 (Fig. 2C). These results showed that Lys-Pg and Lys-plasmin but not Glu-Pg could bind to ADAMTS13. It is known that Glu-Pg and Lys-Pg have different conformational states in solution (*26*). We assumed that immobilized Glu-Pg had, in part, the conformational change on the plate surface. Microheterogeneity of Pg with or without carbohydrates attached to Asn289 is known (*27*). Doublets of Glu-Pg and Lys-Pg shown in Fig. 2 are likely explained by the carbohydrate difference.

Pg-binding domains in ADAMTS13

Because the C and S domains of ADAMTS13 were used as the bait, the Pg-binding regions would reside in the C and S domains. The co-immunoprecipitation analysis using MD-FLAG and MDTCS-FLAG of ADAMTS13 indicated that both could bind to Lys-Pg but not to Glu-Pg (Fig. 3A). The intensity of bound Lys-Pg was apparently lowest in MD-FLAG and highest in full-length ADAMTS13-FLAG, indicating the gradual loss of affinity in domain truncation. The dose-dependent binding experiments showed that Lys-Pg bound to MDTCS-FLAG at a lower concentration (4 nM) than MD-FLAG (Fig. 3B). Although the Lys-Pg binding to MDTCS-FLAG was saturated at 40 nM, the binding to MD-FLAG was not saturated at the same concentration. The results of the yeast two-hybrid screen and the co-immunoprecipitation

analysis together revealed that the C and S domains in ADAMTS13 are necessary for strong binding to Lys-Pg. Because the M domain of ADMATS13 has two glycosylation sites (*28*), doublets of MD-FLAG might be caused by the difference of carbohydrate. Alternatively, we cannot exclude the possibility of limited proteolysis of MD-FLAG.

ADAMTS13-binding region in Lys-Pg

Elastase has been used for the domain isolation of Pg (*23*), and the resulting fragments containing kringle 1 and 4 domains can bind to lysine-Sepharose. We digested Pg with elastase and unbound and bound fractions for lysine-Sepharose were obtained. Lys-Pg, elastase-digested Lys-Pg and lysine-Sepharose unbound and bound fractions of elastase-digested Lys-Pg were subjected to SDS–PAGE (Fig. 4A) for the far-western blotting using ADAMTS13 as the ligand (Fig. 4B). As a result, ADAMTS13 bound to three bands: Lys-Pg, a 40-kDa fragment and a 32-kDa fragment (Fig. 4B, right). N-terminal sequence analysis revealed that the lysine-Sepharose bound 40-kDa fragment was the kringle 4 and 5 and protease domains (K4-K5-P) and the lysine-Sepharose unbound 32-kDa fragment was mini-Pg, which consists of the kringle 5 and protease domains (K5-P). Thus, we concluded that ADAMTS13 bound to mini-Pg but not to the kringle 1–4 domains. This was compatible with the result of the yeast two-hybrid screen that the positive clone contained C-terminal 150 residues of the protease domain of Pg.

Binding of Pg to immobilized ADAMTS13 using Biacore

ADAMTS13 was immobilized on the sensor chip, and the binding of Glu-Pg or Lys-Pg to ADAMTS13 was measured by recording the changes in surface plasmon resonance upon injection of Pgs using Biacore. We observed that Lys-Pg bound to immobilized ADAMTS13 in the dose-dependent manner (Fig. 5A), whereas Glu-Pg could not significantly bind to ADAMTS13 (Fig. 5B). Lys-Pg exhibited a higher binding affinity to ADAMTS13 with a K_d of $1.9 \pm 0.1 \times 10^{-7}$ M (the mean ± SD) than Glu-Pg with a K_d of $5.5 \pm 2.7 \times 10^{-6}$ M (the mean ± SD).

Plasmin and ADAMTS13 activities in the complex

The C and S domains of ADAMTS13 were necessary for the recognition and cleavage of VWF. Therefore, the Lys-Pg binding to ADAMTS13 may affect the ADAMTS13 activity. We examined the effects of Lys-Pg on the ADAMTS13 activity. We found that Lys-Pg did not affect the ADAMTS13 activity towards the natural substrate VWF (Fig. 6A) and the synthetic

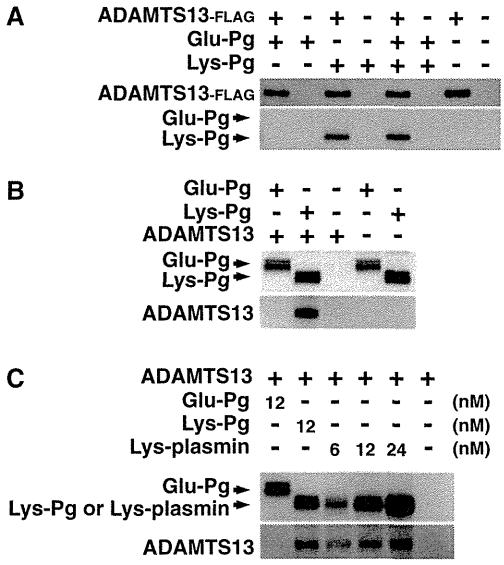

Fig. 2 Binding of ADAMTS13 to Lys-Pg. (A) Co-immunoprecipitation using anti-FLAG mAb. The culture medium containing ADAMTS13-FLAG was incubated with Glu-Pg (100 nM) and/or Lys-Pg (100 nM), and then anti-FLAG mAb-immobilized gel was added to recover bound complexes. Proteins in the complexes were subjected to SDS–PAGE for western blotting using anti-FLAG mAb or anti-Pg mAb. The result is representative of three experiments. (**B** and **C**) Co-immunoprecipitation using anti-Pg mAb. (B) Purified ADAMTS13 (6.7 nM) was incubated with Glu-Pg (12 nM) or Lys-Pg (12 nM), and then anti-Pg mAb was added. Immunocomplexes were subjected to SDS–PAGE for western blotting using anti-Pg mAb or anti-ADAMTS13 mAb WH10. (C) Binding of ADAMTS13 to active-site inhibited plasmin. ADAMTS13 (6.7 nM) was first incubated with Glu-Pg (12 nM), Lys-Pg (12 nM) and APMSF-treated plasmin (6, 12 and 24 nM) and then incubated with anti-Pg mAb. The immunocomplexes were analysed as described in (B). The result is representative of three experiments.

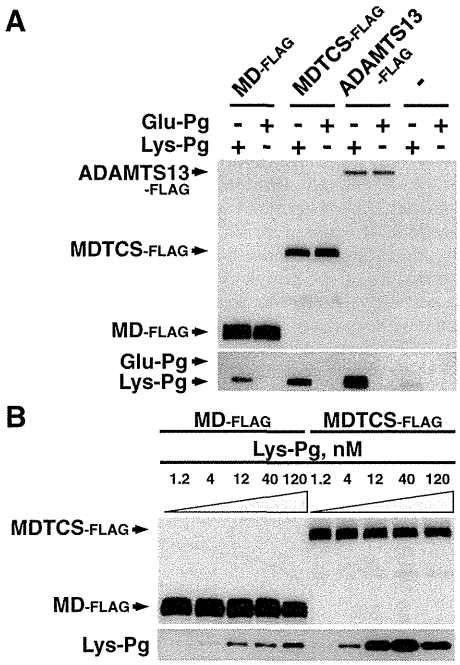

Fig. 3 Binding of ADAMTS13 and its truncated mutants to Glu-Pg or Lys-Pg. (A) Binding of MD-FLAG, MDTCS-FLAG and ADAMTS13-FLAG to Glu-Pg and Lys-Pg. The culture medium containing MD-FLAG, MDTCS-FLAG or ADAMTS13-FLAG was incubated with Glu-Pg (35 nM) or Lys-Pg (35 nM). The complex was immunoprecipitated and then probed with anti-FLAG mAb or anti-Pg mAb. The result is representative of three experiments. (**B**) Dose-dependent binding of Lys-Pg to MD-FLAG and MDTCS-FLAG. Lys-Pg (1.2, 4, 12, 40, 120 nM) was incubated with the culture medium containing MD-FLAG or MDTCS-FLAG. The complex was analysed as described in (A). The result is representative of three experiments.

substrate FRETS-VWF73 (Fig. 6B). The plasmin activity was also not affected by ADAMTS13 even in the 10-fold molar excess of plasmin concentration (Fig. 6C).

Discussion

In this study, we have demonstrated that ADAMTS13 binds to Lys-Pg, the N-terminal truncated form of Pg. This interaction was firstly identified by yeast two-hybrid screen of human liver and brain cDNA libraries using the C and S domains of ADAMTS13 as the bait. This interaction was further demonstrated by the co-immunoprecipitation analysis, the far-western blotting and the Biacore system.

Under physiological conditions, Lys-Pg and Lys-plasmin are not present in circulating blood (*29*). However, in patients undergoing thrombolytic therapy using tissue plasminogen activator, low, but significant, amount of Lys-Pg was detected (*29*). Tissue plasminogen activator can be released from endothelium storage upon venous occlusion, stimulation of epinephrine or desmopressin acetate, and physical exercise. Therefore, under these conditions, Lys-Pg may be locally generated by tissue plasminogen activator and the complex of ADAMTS13 with Lys-Pg might be locally formed, thereby regulating the thrombus formation through VWF cleavage and fibrin degradation.

Physical properties of Glu-Pg and Lys-Pg are quite different. Analysis using small-angle scattering revealed that Glu-Pg has a form with the overall shape of a prolate ellipsoid by interaction between the domains in Pg (*26*). ADAMTS13 can exclusively bind to Lys-Pg but not to Glu-Pg, indicating that ADAMTS13 distinguishes the specific conformation of Lys-Pg. It is known that the conformation of plasmin is resembled to that of Lys-Pg but not Glu-Pg. It is consistent with our result that not only Lys-Pg but also Lys-plasmin can bind to ADAMTS13. Quite recently, the crystal structure of human Glu-Pg has been determined (*30*). The structure clearly showed that seven domains consisting of a Pan-apple domain, five kringle domains and a serine protease domain are loosely clustered in a diamond-shaped zig-zag assembly. Notably, the serine protease domain has a contact with kringle 2 and 4 domains. Although the structure of Lys-Pg remains to be determined, these domain contacts may differ between Glu-Pg and Lys-Pg, resulting in preferable binding of ADAMTS13 to Lys-Pg.

Recently, it was shown that ADAMTS13 is a substrate of plasmin *in vitro* (*31*, *32*). We performed a preliminary experiment as to the ADAMTS13 cleavage with plasmin (data not shown). We found that plasmin cleaved ADAMTS13 into several fragments, and the profile of those fragments was very similar to those previously reported by Crawley *et al.* (*31*) and Hiura *et al.* (*32*). Previous studies showed that the ADAMTS13 activity was progressively decreased by plasmin digestion (*31*, *32*). As for the cleavage sites, plasmin cleaved three peptide bonds, R257-A258 in the metalloprotease domain, R888-T889 in the T4 domain and R1176-R1177 in the T8 domain, but it did not cleave any peptide bonds in the C and S domains

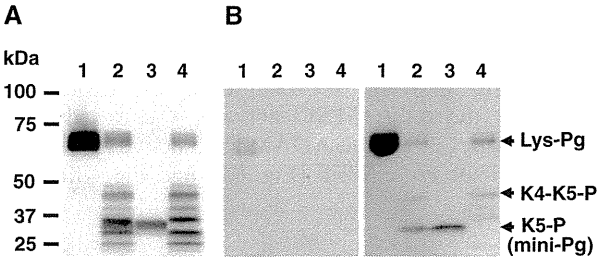

Fig. 4 Binding of ADAMTS13 to mini-Pg. Lys-Pg (lane 1, 1.28 μg protein), elastase-digested Lys-Pg (lane 2, 1.28 μg protein), and lysine-Sepharose unbound (mini-Pg, lane 3, 0.64 μg protein) and bound (several fragments containing kringle 1–4 domains, lane 4, 1.28 μg protein) fractions of elastase-digested Lys-Pg were subjected to SDS-PAGE and transferred onto polyvinylidene difluoride membranes. (A) Coomassie Brilliant Blue staining for N-terminal sequence analysis. The N-terminal sequences of 32-kDa (lane 3) and 40-kDa (lane 4) bands were $V^{461}APPP^{465}$ and $V^{374}QDXY^{378}$, respectively, indicating that those were mini-Pg (K5-P) and a fragment consisting of the kringle 4 and 5 and protease domains (K4-K5-P), respectively. (**B**) Far-western blotting. The membrane was incubated without (left) or with (right) ADAMTS13 (4.5 μg/ml). Bound ADAMTS13 was detected by the HRP-conjugated anti-ADAMTS13 polyclonal antibody. The result is representative of three experiments.

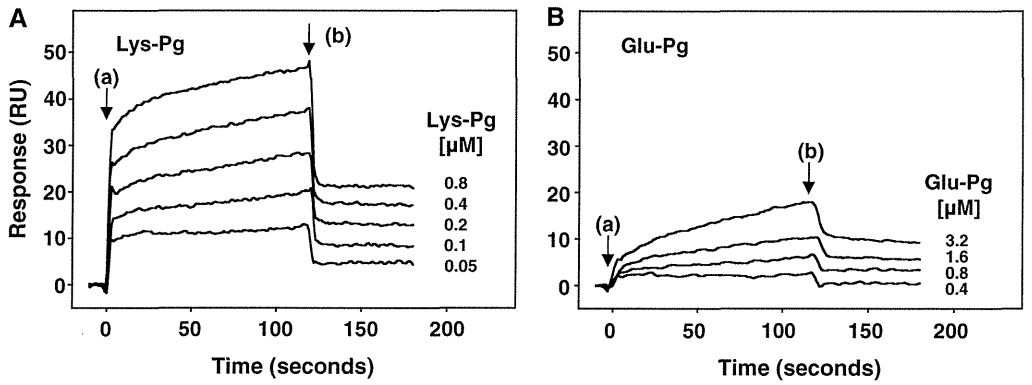

Fig. 5 Binding of Lys-Pg and Glu-Pg to immobilized ADAMTS13 using Biacore. ADAMTS13 was immobilized onto the sensor chip, and Lys-Pg (**A**: 0.05, 0.1, 0.2, 0.4 and 0.8 μM) or Glu-Pg (**B**: 0.4, 0.8, 1.6 and 3.2 μM) was injected over the ADAMTS13-immobilized sensor chip at a flow rate of 20 μl/min for 2 min. The *arrows* indicate the beginning (a) and the end (b) of the application of Pgs. Sensorgrams are shown from a typical experiment, which was repeated at least three times with similar results.

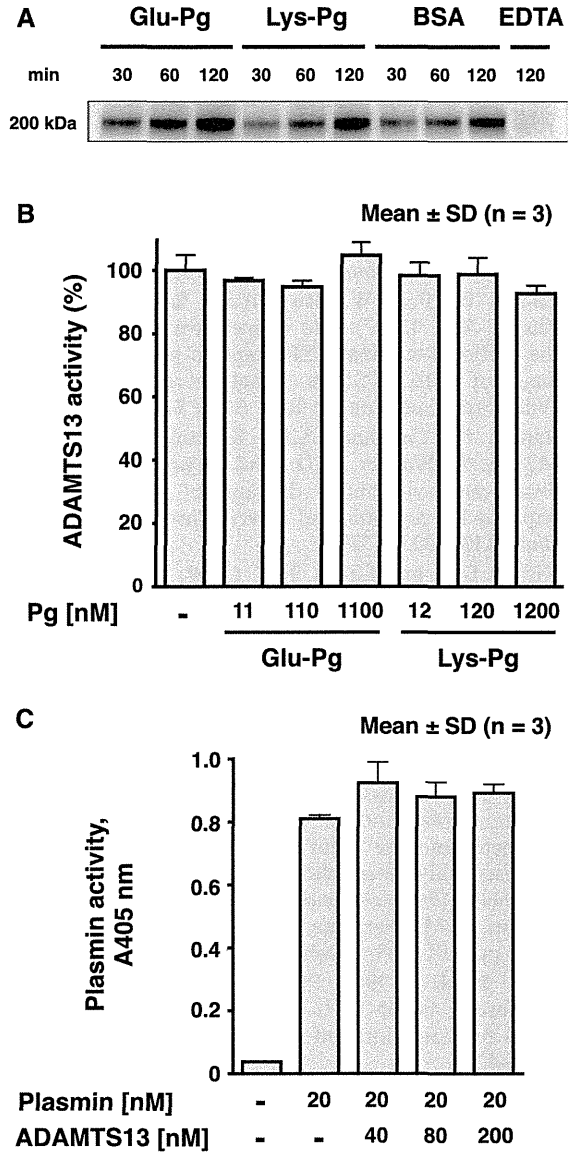

Fig. 6 Plasmin and ADAMTS13 activities in the complex. ADAMTS13 activity was assessed by the appearance of a 200-kDa fragment of VWF using western blotting (**A**) and by FRETS-VWF73 (**B**) as described under the 'Materials and Methods' section. Briefly, for VWF assay, ADAMTS13 was mixed with Glu-Pg, Lys-Pg or BSA and incubated with guanidine-pretreated VWF multimers at 37°C. The cleaved fragment was assessed by western blotting using HRP-conjugated anti-human VWF polyclonal antibody. For FRETS-VWF73 assay, ADAMTS13 was mixed with Glu-Pg or Lys-Pg and was incubated with FRETS-VWF73. Increase in fluorescence was measured with 340-nm excitation and 450-nm emission. The reaction rate was calculated by linear regression analysis of fluorescence over time from 0 min to 10 min. The relative activities were estimated from the activity of ADAMTS13 without Glu-Pg or Lys-Pg. The plasmin activity was assessed using S-2251 as substrate (C) as described under the 'Materials and Methods' section. Briefly, plasmin was preincubated with ADAMTS13 followed by the addition of S-2251. Plasmin activity was recorded as a change in absorbance at 405 nm during 30 min.

(*32*). Therefore, the fragments generated from plasmin-digested ADAMTS13 are likely to have intact C and S domains that are necessary for the plasminogen binding.

Fibrin and endothelial proteins, annexin II and α-enolase, bind to Lys-Pg through its lysine-binding site in the kringle domains (*33*, *34*). Since Lys-Pg can bind to cultured endothelial cells in a rapid and reversible fashion via the lysine-binding sites, annexin II and α-enolase are thought to be endothelial receptors for Pg. Interestingly, ADAMTS13 binds to the elastase fragment consisting of the kringle 5 and the serine protease domain of Lys-Pg. Taken together with the result of yeast two-hybrid screen, our observations suggest that the Lys-Pg binding to ADAMTS13 is a novel binding mechanism through the serine protease domain of Lys-Pg. Since the binding site of Lys-Pg to ADAMTS13 is different from that of Lys-Pg to fibrin or endothelial cells, the ADAMTS13–Lys-Pg complex might be anchored to the cells through the kringle domains of the complex. Additionally, we have demonstrated that ADAMTS13 is still active after the complex is formed. Recently, it has been shown that binding of ADAMTS13 to endothelial cells enhances its enzymatic activity (*35*).

In this study, we demonstrated ADAMTS13 binding to Lys-Pg. The physiological role of this binary complex is not clear at present; however, it might contribute to localize these two proteases at sites of thrombus formation or vascular injury where the fibrinolytic system is activated.

Acknowledgements

We thank Miyuki Kuroi for her excellent technical assistance. We thank Dr. T. Koide at University of Hyogo for human histidine-rich glycoprotein and Dr. I. Ohkubo at Shiga University of Medical Science for human zinc-α2-glycoprotein.Y.S. designed and performed research, analysed and interpreted data, and wrote the paper; K.K. interpreted data; M.A. and K.S. contributed the substantial experimental materials; T.M. designed research, interpreted data and wrote the paper.

Funding

This work was supported in part by a Grant-in-Aid for scientific research from the Ministry of Health, Labor and Welfare of Japan (to T.M.); the Ministry of Education, Culture, Sports, Science and Technology of Japan (to K.K., M.A. and T.M.); and the Program for Promotion of Fundamental Studies in Health Sciences of the National Institute of Biomedical Innovation (NIBIO) of Japan (to T.M.). Shin was a research resident supported by the Japan Health Sciences Foundation at the National Cerebral and Cardiovascular Center Research Institute.

Conflict of interest

K.S. is an employee of Chemo-Sero-Therapeutic Research Institute. The National Cerebral and Cardiovascular Center where T.M. and K.K. (inventors) belong has an awarded patent on the use of reagent, FRETS-VWF73. The other authors state that they have no conflict of interest.

References

1. Moake, J.L. (1998) Moschcowitz, multimers, and metalloprotease. *N. Engl. J. Med.* **339**, 1629–1631
2. Tsai, H.M. (2006) Current concepts in thrombotic thrombocytopenic purpura. *Annu. Rev. Med.* **57**, 419–436
3. Miyata, T., Kokame, K., Banno, F., Shin, Y., and Akiyama, M. (2007) ADAMTS13 assays and

ADAMTS13-deficient mice. *Curr. Opin. Hematol.* **14**, 277–283

4. Hughes, C., McEwan, J.R., Longair, I., Hughes, S., Cohen, H., Machin, S., and Scully, M. (2009) Cardiac involvement in acute thrombotic thrombocytopenic purpura: association with troponin T and IgG antibodies to ADAMTS 13. *J. Thromb. Haemost.* **7**, 529–536
5. Soejima, K., Mimura, N., Hirashima, M., Maeda, H., Hamamoto, T., Nakagaki, T., and Nozaki, C. (2001) A novel human metalloprotease synthesized in the liver and secreted into the blood: possibly, the von Willebrand factor-cleaving protease? *J. Biochem.* **130**, 475–480
6. Zheng, X., Chung, D., Takayama, T.K., Majerus, E.M., Sadler, J.E., and Fujikawa, K. (2001) Structure of von Willebrand factor-cleaving protease (ADAMTS13), a metalloprotease involved in thrombotic thrombocytopenic purpura. *J. Biol. Chem.* **276**, 41059–41063
7. Levy, G.G., Nichols, W.C., Lian, E.C., Foroud, T., McClintick, J.N., McGee, B.M., Yang, A.Y., Siemieniak, D.R., Stark, K.R., Gruppo, R., Sarode, R., Shurin, S.B., Chandrasekaran, V., Stabler, S.P., Sabio, H., Bouhassira, E.E., Upshaw, J.D. Jr, Ginsburg, D., and Tsai, H.M. (2001) Mutations in a member of the ADAMTS gene family cause thrombotic thrombocytopenic purpura. *Nature* **413**, 488–494
8. Soejima, K., Matsumoto, M., Kokame, K., Yagi, H., Ishizashi, H., Maeda, H., Nozaki, C., Miyata, T., Fujimura, Y., and Nakagaki, T. (2003) ADAMTS-13 cysteine-rich/spacer domains are functionally essential for von Willebrand factor cleavage. *Blood* **102**, 3232–3237
9. Zheng, X., Nishio, K., Majerus, E.M., and Sadler, J.E. (2003) Cleavage of von Willebrand factor requires the spacer domain of the metalloprotease ADAMTS13. *J. Biol. Chem.* **278**, 30136–30141
10. Gao, W., Anderson, P.J., and Sadler, J.E. (2008) Extensive contacts between ADAMTS13 exosites and von Willebrand factor domain A2 contribute to substrate specificity. *Blood* **112**, 1713–1719
11. de Groot, R., Bardhan, A., Ramroop, N., Lane, D.A., and Crawley, J.T. (2009) Essential role of the disintegrin-like domain in ADAMTS13 function. *Blood* **113**, 5609–5616
12. Zanardelli, S., Chion, A.C., Groot, E., Lenting, P.J., McKinnon, T.A., Laffan, M.A., Tseng, M., and Lane, D.A. (2009) A novel binding site for ADAMTS13 constitutively exposed on the surface of globular VWF. *Blood* **114**, 2819–2828
13. Feys, H.B., Anderson, P.J., Vanhoorelbeke, K., Majerus, E.M., and Sadler, J.E. (2009) Multi-step binding of ADAMTS-13 to von Willebrand factor. *J. Thromb. Haemost.* **7**, 2088–2095
14. Akiyama, M., Takeda, S., Kokame, K., Takagi, J., and Miyata, T. (2009) Production, crystallization and preliminary crystallographic analysis of an exosite-containing fragment of human von Willebrand factor-cleaving proteinase ADAMTS13. *Acta. Crystallogr. Sect. F Struct. Biol. Cryst. Commun.* **65**, 739–742
15. Akiyama, M., Takeda, S., Kokame, K., Takagi, J., and Miyata, T. (2009) Crystal structures of the noncatalytic domains of ADAMTS13 reveal multiple discontinuous exosites for von Willebrand factor. *Proc. Natl. Acad. Sci. USA* **106**, 19274–19279
16. Banno, F., Kaminaka, K., Soejima, K., Kokame, K., and Miyata, T. (2004) Identification of strain-specific variants of mouse Adamts13 gene encoding von Willebrand factor-cleaving protease. *J. Biol. Chem.* **279**, 30896–30903
17. Majerus, E.M., Anderson, P.J., and Sadler, J.E. (2005) Binding of ADAMTS13 to von Willebrand factor. *J. Biol. Chem.* **280**, 21773–21778
18. Tao, Z., Peng, Y., Nolasco, L., Cal, S., Lopez-Otin, C., Li, R., Moake, J.L., Lopez, J.A., and Dong, J.F. (2005) Recombinant CUB-1 domain polypeptide inhibits the cleavage of ULVWF strings by ADAMTS13 under flow conditions. *Blood* **106**, 4139–4145
19. Zhang, P., Pan, W., Rux, A.H., Sachais, B.S., and Zheng, X.L. (2007) The cooperative activity between the carboxyl-terminal TSP1 repeats and the CUB domains of ADAMTS13 is crucial for recognition of von Willebrand factor under flow. *Blood* **110**, 1887–1894
20. Banno, F., Chauhan, A.K., Kokame, K., Yang, J., Miyata, S., Wagner, D.D., and Miyata, T. (2009) The distal carboxyl-terminal domains of ADAMTS13 are required for regulation of in vivo thrombus formation. *Blood* **113**, 5323–5329
21. Rijken, D.C. and Lijnen, H.R. (2009) New insights into the molecular mechanisms of the fibrinolytic system. *J. Thromb. Haemost.* **7**, 4–13
22. Soejima, K., Nakamura, H., Hirashima, M., Morikawa, W., Nozaki, C., and Nakagaki, T. (2006) Analysis on the molecular species and concentration of circulating ADAMTS13 in blood. *J. Biochem.* **139**, 147–154
23. Sottrup-Jensen, L., Claeys, H., Zajdel, M., Petersen, T.E., and Magnusson, S. (1978) The primary structure of human plasminogen: isolation of two lysine-binding fragments and one "mini"-plasminogen (MW 38,000) by elastase-catalyzed-specific limited proteolysis *Progress in Chemical Fibrinolysis and Thrombolysis* (Davidson, J.F., Rowan, R.M., Samama, M.M., and Desnoyers, P.C., eds.), pp. 191–209, Raven Press, New York
24. Tsai, H.M. (1996) Physiologic cleavage of von Willebrand factor by a plasma protease is dependent on its conformation and requires calcium ion. *Blood* **87**, 4235–4244
25. Kokame, K., Nobe, Y., Kokubo, Y., Okayama, A., and Miyata, T. (2005) FRETS-VWF73, a first fluorogenic substrate for ADAMTS13 assay. *Br. J. Haematol.* **129**, 93–100
26. Mangel, W.F., Lin, B.H., and Ramakrishnan, V. (1990) Characterization of an extremely large, ligand-induced conformational change in plasminogen. *Science* **248**, 69–73
27. Castellino, F.J. and Powell, J.R. (1981) Human plasminogen. *Methods Enzymol.* **80**, Pt C, 365–378
28. Zhou, W. and Tsai, H.M. (2009) N-Glycans of ADAMTS13 modulate its secretion and von Willebrand factor cleaving activity. *Blood* **113**, 929–935
29. Holvoet, P., Lijnen, H.R., and Collen, D. (1985) A monoclonal antibody specific for Lys-plasminogen. Application to the study of the activation pathways of plasminogen in vivo. *J. Biol. Chem.* **260**, 12106–12111
30. Low, R.H., Caradoc-Davies, T., Cowieson, N., Horvath, A.J., Quek, A.J., Encarnacao, J.A., Steer, D., Cowan, A., Zhang, Q., Lu, B.G., Pike, R.N., Smith, A.I., Coughlin, P.B., and Whisstock, J.C. (2012) The X-ray crystal structure of full-length human plasminogen. *Cell Rep.* **1**, 185–190
31. Crawley, J.T., Lam, J.K., Rance, J.B., Mollica, L.R., O'Donnell, J.S., and Lane, D.A. (2005) Proteolytic inactivation of ADAMTS13 by thrombin and plasmin. *Blood* **105**, 1085–1093

32. Hiura, H., Matsui, T., Matsumoto, M., Hori, Y., Isonishi, A., Kato, S., Iwamoto, T., Mori, T., and Fujimura, Y. (2010) Proteolytic fragmentation and sugar chains of plasma ADAMTS13 purified by a conformation-dependent monoclonal antibody. *J. Biochem.* **148**, 403–411
33. Miles, L.A., Dahlberg, C.M., Plescia, J., Felez, J., Kato, K., and Plow, E.F. (1991) Role of cell-surface lysines in plasminogen binding to cells: identification of alpha-enolase as a candidate plasminogen receptor. *Biochemistry* **30**, 1682–1691
34. Hajjar, K.A., Jacovina, A.T., and Chacko, J. (1994) An endothelial cell receptor for plasminogen/tissue plasminogen activator. *I. Identity with annexin II. J. Biol. Chem.* **269**, 21191–21197
35. Vomund, A.N. and Majerus, E.M. (2009) ADAMTS13 bound to endothelial cells exhibits enhanced cleavage of von Willebrand factor. *J. Biol. Chem.* **284**, 30925–30932

第73回日本血液学会学術集会
シンポジウム6
血栓止血学・血管生物学
の最近の進歩

ADAMTS13研究の最先端

宮田敏行[1]，小亀浩市[1]，秋山正志[1]，坂野史明[1]，
中山大輔[1]，武田壮一[2]

Key words : ADAMTS13, Platelet, Thrombotic thrombocytopenic purpura, Von Willebrand factor

はじめに
血栓性血小板減少性紫斑病とは

血栓性血小板減少性紫斑病（thrombotic thrombocytopenic purpura, TTP）は微小血管内に血小板血栓が生じる致死率の高い疾患である。TTPは血中のフォンビルブランド因子（VWF）切断酵素であるADAMTS13が先天性もしくは後天性の原因により活性が著減し，超高分子量VWFマルチマーが血中に蓄積し，これが引き金となり血小板血栓が形成される。微小血管に血小板血栓ができるため，消費性に血小板数の減少を示し，赤血球が血栓に衝突し損傷を受けるため，破砕赤血球が見られ溶血性貧血を示す。脳の微小血管が閉塞すると虚血性または梗塞性の障害として動揺する精神・神経症状が観察される。また，長期にわたって腎機能障害がみられる。VWFは2,050アミノ酸残基のモノマーがN末端どうし，C末端どうしでジスルフィド結合を介して直鎖状に繋がり，超高分子量マルチマー（unusually large VWF multimer, UL-VWFマルチマー）として合成され血管内皮細胞から血中に分泌される。このUL-VWFマルチマーは血小板活性化能が高く，これが血中に蓄積するTTP患者では，微小血管に血小板血栓が生じる。このTTPの病態は血漿交換により劇的に改善される。これは血漿交換によりADAMTS13に対する抗体が血漿から除去されること，かつADAMTS13が補充されることによる。これにより，ADAMTS13活性が回復し，超高分子量VWFマルチマーが通常のマルチマーまで分解され，血小板血栓の形成が抑制される[1~4]。

先天性ADAMTS13欠損症の遺伝子解析と
ADAMTS13活性測定基質の開発

TTPの原因遺伝子として，血漿メタロプロテアーゼADAMTS13が2001年にクローニングされた[5~7]。私達は奈良県立医科大学藤村吉博教授と共同研究を行い，まず先天性ADAMTS13欠損症の遺伝子解析を行った。その結果，C908Y変異は本州に，R193W変異は瀬戸内地域と東北地方に，Q449Xは東北地方に複数例みられるなど，変異の地理的な分布も示すことができるまでにADAMTS13の遺伝子変異の情報が蓄積された[8,9]。これらの先天性ADAMTS13欠損症のうち幾人かは，妊娠時に先天性ADAMTS13欠損症によるTTPと診断された[10]。また，脳梗塞治療薬として広く用いられていた抗血小板薬チクロピジンの副作用として，極めて頻度は低いがTTPの発症例が報告された[11]。ADAMTS13活性を簡便に測定できればTTPの診断を早期に行えるが，当時は活性測定にSDS-アガロース・抗VWF抗体ウェスタンブロット法を用いていたので数日を要した。そこで私達はADAMTS13の簡易測定法の開発に着手し，VWFのA2ドメイン内の73残基が最小基質であることを明らかにした[12]。その後，切断部位であるTyr1605-Met1606結合をはさみ蛍光基と消光基を導入した蛍光基質FRETS-VWF73を開発した[13]。本基質は蛍光共鳴エネルギー転移により自家蛍光が抑えられているが，ADAMTS13によりTyr1605-Met1606結合が切断されると蛍光を発する。本基質を用いると30分以内にADAMTS13活性を定量できる。

[1]国立循環器病研究センター　分子病態部
[2]国立循環器病研究センター　心臓生理機能部

日本人一般住民を対象にしたADAMTS13活性測定と先天性ADAMTS13欠損症の推定頻度

簡便で定量性のあるADAMTS13活性測定基質を開発したので，本基質を用いて日本人3,616人（男性1,687人，女性1,929人）のADAMTS13活性の測定を行った[14]。ADAMTS13活性は40%から200%程度まで幅広い分布を示した。男性は女性より活性が低いことが判明した（男性，93±24%，平均値±標準偏差，女性，106±27%，P<0.0001）（図1A）。また，30歳台から80歳台までで活性を比較すると，男女ともに加齢により特に60歳以降，活性は低下した（図1B）。80歳台の活性は30歳台の活性の約80%であった。一方，VWF抗原量は加齢により増加するが，今回の集団でもVWF量は加齢により増加し，80歳台のVWF量は30歳台に比べ男性で1.8倍，女性で1.7倍増加していた（図1C）。その結果VWF/ADAMTS13の比は加齢により劇的に増加

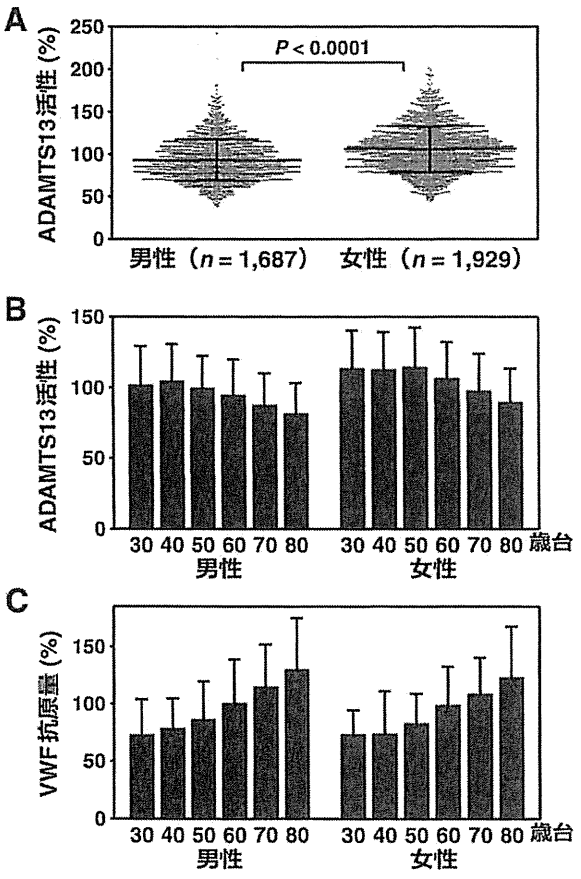

図1 日本人一般住民のADAMTS13活性とVWF抗原量[14]
A. FRETS-VWF73を用いて測定したADAMTS13活性。男性のADAMTS13活性は女性の活性より低い。
B. 年齢別のADAMTS13活性。
C. 性別に分けた年齢別のVWF抗原量。

することが判明した[14]。この比は急性心筋梗塞や肝硬変で上昇するといわれており，高齢者の易血栓性を反映しているものと考えられる。ADAMTS13の活性測定の基質にVWFを用いた場合，検体試料中のVWF濃度が活性に影響することが危惧されていた。しかし，FRETS-VWF73を基質に用いると，ADAMTS13活性は血中VWF濃度に全く影響を受けないことが明らかとなった。また，VWFにはABO型糖鎖が結合しているので，血中VWF濃度はO型で低いことが知られている。私達の測定でも，O型の人のVWF濃度は明らかな低値を示したが，ADAMTS13活性はABO型で影響を受けなかった。

次に一般住民でのADAMTS13活性値を用いて，先天性ADAMTS13欠損症の頻度の推定を行った[15]。一般住民3,200人（男性1,500人，女性1,700人）から，最も活性の低い32人，次いで活性の低い32人，中央値の活性を示す32人，最も活性の高い32人（各群，男性15人，女性17人）合計128人を選び，ADAMTS13の蛋白質コード領域の全塩基配列の決定を行った。その結果，活性最低値群に7つのまれなミスセンス変異・ノンセンス変異・フレームシフト変異，次低値群に3つのまれなミスセンス変異・フレームシフト変異，活性中央値群と活性高値群にそれぞれ2つのまれなミスセンス変異を同定した。この結果から，32人中には活性に影響を与えないまれなミスセンス変異が2つ存在すると考えられた。これを考慮すると，活性最低値群に5アレル，および活性次低値群に1アレルの機能消失を伴なうと考えられる変異アレルが同定されたこととなる。すなわち，対象とした3,200人中に6人（すなわち533人に1人）のADAMTS13欠損症ヘテロ接合体の存在が推定された。この頻度は家族性高脂血症の頻度によく一致する。これより，TTPの発症に繋がるADAMTS13欠損症ホモ接合体もしくは複合ヘテロ接合体の頻度は110万人に1人と推定され，日本人には約110人の先天性ADAMTS13欠損症の存在が推定された[15]。これまでのところ，日本人には43人の先天性ADAMTS13欠損症患者が報告されている[9]。

ADAMTS13の東アジア人特有のミスセンス変異，P475S変異

私達は先天性ADAMTS13欠損症の遺伝子解析を行なう過程で，東アジア人特有のミスセンス変異，P475S，を同定した[8]。日本人約10人に1人が本変異のヘテロ接合体である。一般住民を対象にした研究から，P475S変異ヘテロ接合体はADAMTS13活性が約17%低下していることが判明した[15]。組換え変異体（MDTCS-P475S）は野生型に比べFRETS-VWF73に対してKm値

が2倍大きくなっていたがKcat値は変化しなかった。組換え変異体はずり応力をかけたVWFを切断した。これらの結果より，本変異保有者はADAMTS13活性を保持しており，本変異が直接TTPのリスクにはならないと考えられた。

ADAMTS13によるVWFの切断メカニズム：ずり応力による基質VWFA2ドメインのアンフォールドとADAMTS13による複数のエクソサイトを介した結合

先に述べたように，ADAMTS13による基質VWFの切断にはVWFの73残基が必要であり，より短い64残基にするともはや切断しない。例えば，トロンビンは3残基から成る合成基質を効率良く切断するし，凝固Xa因子は4残基から成る基質を切断する。ADAMTS13が73残基という長いアミノ酸配列を要求することは，これまでの凝固プロテアーゼの基質認識とは異なったメカニズムによる切断が考えられた。そこで，ADAMTS13の立体構造の解析を行った。ADAMTS13は1,427残基で明らかなドメイン構造からなる（図2A）。MDTCS領域は全長ADAMTS13とほぼ同程度の活性を示す[16]。また，SドメインにはADAMTS13の活性中和自己抗体の結合部位の存在が指摘されていた[16]。そこで，MDTCS領域を培養細胞で発現させ結晶化を試みた。しかし，不溶性のため結晶化には至らなかった。そこでDTCS領域の結晶化とその構造解析を行った[17,18]。

ADAMTS13-DTCSはD，C_A，Sという3つの球状ドメインがTとC_Bという長いドメインで連結している構造をとっていた[17]（図2B）。結晶構造解析からCドメインはC_AとC_Bから成ることが判明した。Dドメインはディスインテグリン様構造をとらず，C_Aドメインと似たフォールディングをしていた。後天性TTP患者に見られるADAMTS13の活性阻害自己抗体（抗ADAMTS13抗体）のエピトープがSドメインに報告さ

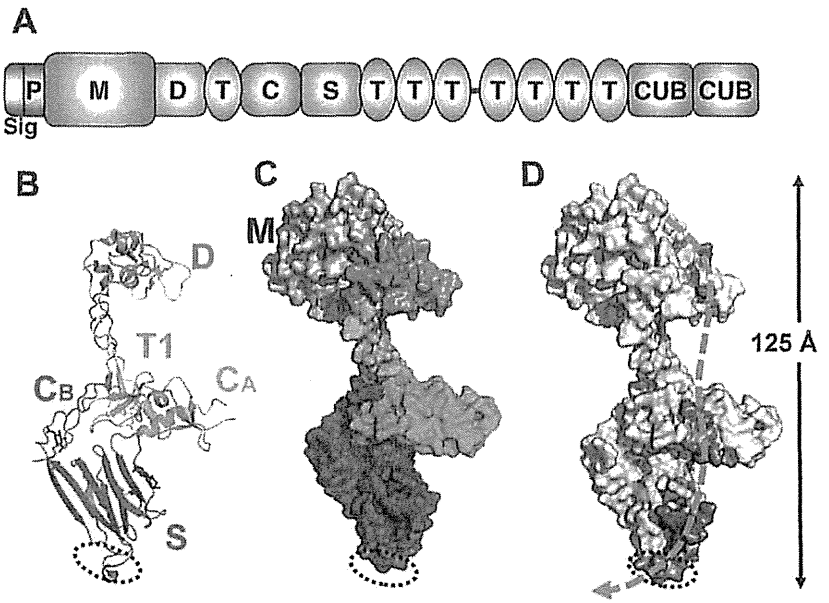

図2 ヒトADAMTS13のドメイン構造と部分立体構造

A. ADAMTS13のドメイン構造。MDTCS領域は全長ADAMTS13とほぼ同等の活性を示す。ADAMTS13は，N末端から，メタロプロテアーゼドメイン（M），ディスインテグリン様ドメイン（D），トロンボスポンジン1 I型リピートドメイン（T），Cys-richドメイン（C），スペーサードメイン（S），7つのTドメイン，2つのCUBドメインから成る。シグナル配列（Sig）とプロ配列（P）は生合成過程で切断される。

B. X線結晶構造解析で決定したADAMTS13のDTCS領域の立体構造[17]。Sドメイン先端の点線で囲んだループ（Arg660，Tyr661，Tyr665を含む）に自己抗体が結合するとTTPを発症する[19]。

C. メタロプロテアーゼ（M）ドメインの構造をモデリングしDTCSに結合させたMDTCSモデル。

D. MDTCS構造中の3つのエクソサイトを赤色および赤茶色で示した。このエクソサイトにVWFの73残基が結合する。基質であるVWFはオレンジ色で示した様にMDTCSに結合すると考えられる。